JOINT INSTITUTE FOR AERONAUTICS AND ACOUSTICS

National Aeronautics and
Space Administration

Ames Research Center

NASA-CR-177328
19850006487

Stanford University

JIAA TR - 52

AN EXPERIMENTAL STUDY OF AIRFOIL-SPOILER AERODYNAMICS

Blair G. McLachlan and K. Karamcheti

NF01716

STANFORD UNIVERSITY
Department of Aeronautics and Astronautics
Stanford, California 94305

APRIL 1984

JIAA TR - 52

AN EXPERIMENTAL STUDY OF AIRFOIL-SPOILER AERODYNAMICS

BLAIR G. MCLACHLAN AND K. KARAMCHETI

APRIL 1984

This Page Intentionally Left Blank

ABSTRACT

Results are presented from an experimental investigation of the steady/unsteady flow field generated by a typical two-dimensional airfoil with a statically deflected flap type spoiler. Subsonic wind tunnel tests were made over a range of parameters: spoiler deflection, angle of attack, and two Reynolds numbers (2.8 and 5.2 $\times 10^5$); and involved comprehensive measurements of the mean and fluctuating surface pressures, velocities in the boundary layer, and velocities in the wake. Also, schlieren flow visualization of the near wake structure was performed.

The mean lift, moment, and surface pressure characteristics are in agreement with previous investigations of spoiler aerodynamics. At large spoiler deflections, boundary layer character affects the static pressure distribution in the spoiler hingeline region; and, the wake mean velocity field reveals a closed region of reversed flow aft of the spoiler.

It is shown that the unsteady flow field characteristics are as follows: One, that the unsteady nature of the wake is characterized by vortex shedding; Two, the character of the vortex shedding changes with spoiler deflection; Three, the vortex shedding characteristics (Strouhal number and base pressure coefficient) are in agreement with other bluff body investigations; Four, the vortex shedding frequency component of the fluctuating surface pressure field is of appreciable magnitude at large spoiler deflections.

The results are presented in light of the consideration that the flow past an airfoil with deflected spoiler is a particular problem in bluff body aerodynamics.

ACKNOWLEDGMENTS

TABLE OF CONTENTS

APPENDICES

LIST OF FIGURES

Appendices

LIST OF TABLES

NOMENCLATURE

b	airfoil span
c	airfoil chord
C_ℓ	airfoil section lift coefficient, section lift/qc
ΔC_ℓ	airfoil section lift increment coefficient, $\{C_\ell - C_{\ell,\delta=0}\}_{\alpha=\text{constant}}$
Cm	airfoil section pitching-moment coefficient, about quarter chord, section moment $/qc^2$
ΔCm	airfoil section pitching-moment increment coefficient, $\{Cm - Cm_{\delta=0}\}_{\alpha=\text{constant}}$
Cp	static pressure coefficient, $(P - P_\infty)/q$
Cpb	base pressure coefficient, $(P_b - P_\infty)/q$
f	vortex shedding frequency, Hz
h	spoiler projection height, vertical distance from spoiler tip to airfoil trailing edge
H	boundary layer shape factor, δ^*/θ
P	static pressure
p	mean-square surface pressure fluctuation
$Prms$	root-mean-square surface pressure fluctuation
q	free stream dynamic pressure, $(1/2)\rho U_\infty^2$
Re	Reynolds number, based on airfoil chord, $U_\infty c/\nu$
$Re_{,h}$	Reynolds number, based on h, $U_\infty h/\nu$

$S_{,c}$	Strouhal number, based on airfoil chord, fc/U_∞
$S_{,h}$	Strouhal number, based on h, fh/U_∞
U	mean velocity
U'_{rms}	root-mean-square velocity fluctuation
X	airfoil chordwise coordinate, measured from leading edge
Y	airfoil spanwise coordinate, measured from midspan
Z	boundary layer coordinate, orthogonal to mean chord line, measured from airfoil surface
α	geometric angle of attack, deg.
δ	spoiler deflection angle from nested position, deg.
$\delta^{\bullet}$	displacement thickness, $\int_0^{Ze} (1 - U/U_e)dZ$
θ	momentum thickness, $\int_0^{Ze} (U/U_e)(1 - U/U_e)dZ$
ϵ	blockage correction factor, $\Delta U_\infty/U_\infty$
ν	kinematic viscosity
ρ	free stream fluid density
ϕ	phase angle delay in one period of vortex shedding, deg.

Subscripts

b	base (region aft of spoiler)
e	edge of boundary layer
∞	free stream

I. INTRODUCTION

Definition: "A spoiler is basically a device that "spoils" the flow about a wing section. . . in such a manner that a lift differential is produced"[1]

"A small plate arranged to project above the upper surface of a wing to disturb the smooth airflow, with consequent loss of lift and increase of drag"[2]

1.1 General Remarks

Spoilers are well known aerodynamic control devices in use on flight vehicles: as lateral controls, lift dumpers, and speed brakes. However, the prediction of spoiler aerodynamic characteristics is still difficult[3]; consequently, the design and development of spoilers depends primarily on extensive wind tunnel testing. In order to efficiently develop theoretical methods that can aid in the design process a fundamental understanding of the spoiler flow field is required. A further stimulus to acquire a basic understanding of the spoiler flow field is the current/future interest in spoilers for active control technology (ACT) applications [3–6] (e.g. flutter suppression, direct force control, gust load alleviation. . .): effective implementation being heavily dependent on the prediction accuracy of spoiler aerodynamic characteristics.

1.2 Nature of Problem

The spoilers in use on modern transport aircraft are of the flap type[1] (see Figure 1.1): basically, this type of spoiler is a panel affixed to the wing upper surface trailing edge region; that when deflected upwards (the panel rotating about its leading edge) causes the flow to separate over the wing surface in a controlled manner producing a lift decrease and a drag increase. Spoiler aerodynamic characteristics are the most difficult of the aircraft control surfaces to predict due to the present general inability to model separated flows.

Spoilers have several features that make them desirable for aircraft lateral control: spoilers produce large rolling moments; spoilers are an alternative to ailerons

---

[1]The term "flap type" is used to denote that this type of spoiler configuration is equivalent to a split-flap mounted on the upper (suction) side of an airfoil.

for full roll control, permitting the use of full span flaps, with obvious STOL applications and advantages (already in limited general aviation use, e.g., Mitsubishi MU-2); spoilers produce a favorable yawing moment, unlike ailerons that produce an adverse yawing moment.[2] Also, at high speeds, spoilers in comparison to ailerons, are usually more effective, and are much less likely to suffer from aeroelastic effects (i.e. control reversal).

Unfortunately, the full potential of spoilers as lateral controls has not been realized due to some of the aerodynamic features they display:

- Spoilers display non-linear control effectiveness: the lift reduction is a non-linear function of the spoiler deflection. This non-linearity is particularly pronounced when spoilers are used in the presence of a deflected flap. An illustration of this non-linearity for a typical transport aircraft is displayed in Figure 1.2. This is a serious weakness of spoilers causing an increased complexity of the aircraft control system to integrate the spoilers with the other control surfaces (e.g. ailerons) to provide linear control (necessary to satisfy the pilot and autopilot functions). Historically, this characteristic has limited attaining one of the advantages listed previously: the use of spoilers for full roll control in the presence of full span flaps.

- The turbulent wake that results when the spoiler is deflected is highly unsteady and through interaction with the horizontal tail or the wing itself can cause buffet[*].

- A time delay exists between the spoiler deflection and the reduction in lift; consequently, the aircraft response.

- Unacceptable pitching-moments can be caused due to the change in the wing pitching-moment with spoiler deflection, and the influence of the spoiler wake on the horizontal tail.

---

[2]Interestingly, it is possible for spoilers to produce an adverse yawing moment under certain conditions (see Hoerner et al.[1,pg.10-20]).

[*]An aerodynamic induced vibration.

2

Reviews that cover spoiler performance and design aspects are given by Hoerner et al.[1], Siddalingappa et al.[7], and Mack et al.[8].

A considerable amount of data exists on spoiler performance for design purposes. However, since this data base concentrates on overall aircraft performance it provides little understanding of the fundamental nature of the spoiler flow field. The present experimental study is an attempt to obtain such a fundamental understanding.

In practice spoiler aerodynamic characteristics depend on Reynolds number, Mach number, angle of attack, wing airfoil section, spoiler profile and location, and on the numerous geometrical details of the aircraft configuration, e.g., wing sweep and aspect ratio, the presence of high lift devices and other control surfaces, - - -, etc.. To make the present study tractable it is confined to a two-dimensional airfoil-spoiler configuration, to static spoiler deflections, and to one spoiler location. The section of the configuration is typical of modern transport aircraft. In addition, the present study is further confined to low speeds, to two Reynolds numbers, and to selected values of angle of attack. A description of the experiment is provided in chapter two.

1.3 Historical Perspective

Historically, interest in spoilers was initially as lateral control devices[3], and dates back to the early days of NACA; a review of this research is provided by Weick et al.[9,10]. The bulk of the data from then till recently is confined to the global mean quantities: surface pressures, forces, and moments. Due to the complex nature of the spoiler flow field such information guides theoretical formulation in a limited way. Only recently have efforts been made to obtain information on the overall flow field structure generated by spoilers. A comprehensive review of this work and the earlier experimental and theoretical efforts is given by Mack et al.[8] and Siddalingappa et al.[7].

The information that exists in the literature on the overall flow field structure

---

[3]The impetus for this initial interest was the recognition that spoilers offered a means of lateral control permitting the use of full span flaps.

3

of spoilers concentrates on the steady flow field of a two-dimensional airfoil-spoiler-flap configuration (see Mack et al.[8]): this configuration is of primary interest due to the pronounced non-linear aerodynamic characteristics that spoilers display in the presence of a deflected flap. The detailed characteristics of the flow field of an airfoil-spoiler alone have been hypothesized by Mack et al.[8]. However, little experimental information exists on the details of the flow field structure of this configuration – especially scarce is information on the unsteady flow field: the literature being confined to a few spectra of the wake velocity fluctuations (see Wentz et al.[11]).

1.4 Present Investigation

This dissertation presents the results of an experimental study of the steady/unsteady flow field generated by a two-dimensional airfoil with a statically deflected flap type spoiler. The investigation was exploratory in nature, designed to gain a physical insight into the flow field of a typical transport airfoil-spoiler configuration, and provide a data base for the validation of computational models. Tests involving comprehensive measurements of the mean and fluctuating surface pressures, velocities in the boundary layer, and velocities in the wake were carried out over a two-dimensional airfoil-spoiler configuration. Also, schlieren flow visualization of the near wake structure was performed. This study is part of a larger program, a cooperative effort between the Boeing Company and Stanford University, into the aerodynamics of spoilers. Results of this research program have been presented previously: Ayoub et al.[12], and McLachlan et al.[13].

1.5 Report Outline

A brief outline of the remainder of this report follows.

Chapter II describes the experiment; for the sake of brevity details of the experiment are relegated to the appendices.

Chapter III presents the experimental results. This chapter is divided into two parts: the mean flow field and unsteady flow field measurements being dealt with separately.

4

Chapter IV gives a summary of the conclusions and recommendations for further research.

II. DESCRIPTION OF EXPERIMENT

2.1 Wind Tunnel

The experiments were performed in the 18 x 18 inch (45.72 x 45.72 cm)[4] rectangular closed circuit low speed wind tunnel in the Department of Aeronautics and Astronautics of Stanford University (see Figure 2.1). A detailed description of the wind tunnel and its characteristics is given by Smith et al.[14] and Digumarthi et al.[15]. Reference may be made to Appendix A for a description of the test section and probe traversing mechanism used for the tests.

2.2 Model(s)

The airfoil section tested is that of a Boeing research airfoil (see Figure 2.2) of 8 inch (20.32 cm) chord. It has a spoiler .1554 chords long hinged at .733 chords.

Three aluminum two-dimensional models, horizontally spanning the test section, were tested, each dedicated to a particular measurement: Model no. 1 was used for the velocity measurements in the surface shear layers and wake, and unsteady schlieren flow visualization of the near wake structure; Model no. 2 was used for surface static pressure measurements; Model no. 3 was used for fluctuating surface pressure measurements.

Reference may be made to Appendix B for a detailed description of the models construction and mounting in the test section; and to Appendix D for a detailed description of the models instrumentation. In the rest of the report no distinction will be made between models 1, 2, and 3: the singular term model (or airfoil) will be used.

2.3 Test Conditions

Measurements of static and fluctuating pressure on the surface, velocity in the boundary layer, and velocity in the wake were made over the following range of parameters: spoiler deflection (0° to 60°), angle of attack (−8° to 18°), and two Reynolds numbers (2.8 and 5.2 $\times 10^5$). Table 2.1 lists the operating conditions for

[4]test section size

6

Table 2.1 Test Conditions

	Surface Static Pressure	Boundary Layer (hot-wire)	Wake Mean Velocity Field (dual split-film)	Unsteady Surface Pressure (kulite)	Near Wake Flow Visualization (schlieren)
$Re(x\ 10^5)$	2.8 & 5.2	2.8 & 5.2	2.8	2.8 & 5.2	2.3
δ, deg.	0°, 15°, 30°, 60°	0°, 15°, 30°, 60°	15°, 30°, 60°	0°, 5°, 15°, 20°, 30°, 45°, 60°	15°, 30°, 60°
α, deg.	-8° to 18°	0°	0°	-4° to 16°	0°

Note: Mach no. < .12 over all test conditions.

each type of measurement made. Also, schlieren flow visualization of the near wake structure was performed for a range of spoiler deflections (15°, 30° and 60°), 0° angle of attack, and a Reynolds number of 2.3 $\times 10^5$.

2.4 Boundary Layer Trip

A boundary layer trip consisting of a spanwise strip of randomly distributed .01 inch diameter glass beads was located between chordwise locations of 5 to 7.5%. Effectiveness of the trip in promoting turbulence ahead of the spoiler depended upon the Reynolds number (free stream velocity), spoiler deflection, and the angle of attack. Only for the highest Reynolds number tested and positive angles of attack was the trip effective in promoting turbulence over all the spoiler deflections tested. Outside this range of parameters the boundary layer ahead of the spoiler hingeline was of a transitional nature (close to laminar).

2.5 Instrumentation (General Description)

A general description of the instrumentation employed for the tests will be given here: for a detailed description reference may be made to Appendix D.

Chordwise and spanwise rows of static pressure holes (84 total) were distributed over the upper and lower surface of the airfoil. The static pressure was measured with a (96 port, 4 transducer) scanivalve.

Velocity measurements, mean and r.m.s., in the boundary layer were made using a single channel hot-wire anemometer with linearizer. Hot-wire traverses, in a vertical path, were made at the airfoil midspan (i.e. in the x-z plane).

Velocity measurements in the wake were performed using dual split film anemometry. This method allows accurate velocity measurements in regions of reversed flow. Measurements were also made in the boundary layer; however, due to the size of the sensor in relation to the boundary layer the results are only qualitative. The Boeing Company designed this instrumentation and performed this phase of the test at Stanford University.

Fluctuating surface pressures were measured using unsteady pressure transducers

8

(11 total) distributed in a midspan chordwise row over the upper and lower surface of the airfoil.

Flow visualization of the near wake structure was performed using the schlieren method; this work was carried out by the authors co-workers (Dr. S. Bodapati and G. Hadjidakis).

2.6 Data Reduction (General Description)

Only a general description of the data analysis will be provided in this section: reference may be made to Appendix E for details.

Data from the static surface pressure, boundary layer velocity survey, and wake velocity survey was processed into engineering units and coefficient form using a micro-computer. The sectional lift and moment coefficients were found by numerically integrating the midspan chordwise static pressure distribution. Boundary layer characteristics (δ^*, θ, and H) were calculated from the hot-wire mean velocity profiles in the standard fashion (refer to Appendix E-1.2). Since the hot-wire measurements are not valid in regions of reversed flow, the calculations are only approximate where the boundary layer has separated. Separation of the boundary layer was indicated by visual inspection of the mean velocity profiles and the magnitude of the shape factor: according to von Doenhoff et al.[16] separation of a turbulent boundary layer occurs for values of the shape factor (H) greater than 1.8 and less than 2.6. Time series analysis of the fluctuating surface pressure, boundary layer velocity survey, and wake velocity survey data was performed using a fast Fourier transform analyzer and a direct computation correlator.

2.7 Blockage Corrections

Except where mentioned, no blockage corrections were applied to the data. When applied, the method of Allen and Vincenti[17] was used for calculation. The drag coefficient values used in the calculation came from data supplied by the Boeing Company. Blockage correction factors (ϵ) were estimated (see Table 2.2), for an angle of attack of 0°, to vary from .01 to .05, corresponding to spoiler deflections of 0° to 60°, respectively.

In the present study it is assumed that the presence of the test section walls does not alter the physics of the flow field structure. Of note, is that wall interference can affect the separation mechanism and wake structure of bluff bodies, such as circular cylinders. Wall interference should have little influence on the wake structure of the airfoil-spoiler configuration, since the boundary layer separation points are fixed at the spoiler tip and the airfoil trailing edge. However, the boundary layer separation and reattachment points in the spoiler hingeline region are not fixed; therefore, wall interference could influence the separation/reattachment mechanism in that region. Also, at large negative angles of attack the lower surface separation point does not remain fixed at the airfoil trailing edge but moves forward on the lower surface; therefore, at large negative angles of attack, wall interference could influence the separation mechanism on the lower surface.

Table 2.2

Blockage Correction Factors
$\alpha = 0°$

δ (deg)	ε
0	.0099
5	.0103
15	.0130
20	.0149
30	.0208
45	.0312
60	.0488

III. Experimental Results

3.1 General Remarks

A two-dimensional airfoil with a deflected spoiler generates a wake that displays features characteristic of bluff bodies: separation of the boundary layer on either side of the body; the interaction of the free shear layers and the formation of vortices. In the time averaged picture of the flow field this process results in a large wake that considerably modifies the potential pressure distribution by displacing the outer flow streamlines[1]. A salient feature of bluff body flows is that the near wake structure essentially determines the outer flow, and therefore the pressure distribution over the body: the term "near wake" denotes the vortex formation region, that is, the region from the separation points to the establishment of the vortices. The aim here is to point out that the spoiler generated near wake structure determines the aerodynamic performance of the airfoil-spoiler configuration.

It is not appropriate here to provide a discourse on bluff body aerodynamics (review articles on this subject are provided by Morkovin [18] and Berger et al[19]), only to note that bluff body aerodynamic studies of a fundamental nature provide information useful in understanding spoiler aerodynamics. In particular, the bluff body studies of Roshko[20,21] provide insight into the importance of the vortex formation process in setting the near wake structure and thereby the overall flow[2]. In the presentation of the experimental results concepts from Roshko's work will be introduced where appropriate.

The description of the spoiler flow field characteristics is presented in two parts: first, the mean flow field characteristics; second, the unsteady flow field characteristics. However, even though the mean and unsteady flow field characteristics are presented separately they should not be viewed as being independent of one another. For the mean flow field is nothing more than the time average of the unsteady flow field.

---

[1]This study does not consider the thin wake case: the wake generated at small spoiler deflections (<5°), where the boundary layer separates from the spoiler tip and reattaches on the airfoil upper surface before the trailing edge.

[2]Also of mention—as Roshko[20,21] points out—are the classic bluff body studies of Fage et al.[22,23].

3.2 Mean Flow Field Characteristics

3.2.1 Lift, Moment, and Static Surface Pressure

The lift characteristics are shown in Figure 3.1. At a fixed spoiler deflection the lift increases in the usual manner with angle of attack; at a fixed angle of attack the lift decreases with increasing spoiler deflection. The slope of the lift curve with angle of attack, for different spoiler deflections, remains approximately constant, indicating it to be independent of spoiler deflection: the lift curve slope values ranged from .114/deg to .119/deg, corresponding to spoiler deflections of 0° to 60°, respectively; these lift curve slope values are in fair agreement with the value of .110/deg derived from two-dimensional thin airfoil theory. Slight variation in the lift coefficient is displayed between the two Reynolds numbers tested. Also, from the lift curve it appears that the maximum lift and the stall angle of attack increase as the spoiler deflection increases: however, due to wall interference at such large angles of attack no conclusions can be drawn from that region of the lift curve.

The lift increment (the lift change due to spoiler deflection) as a function of spoiler deflection is a measure of control effectiveness; this increment is shown in Figure 3.2 for the highest Reynolds number tested. For moderate angles of attack (0° to 8°) the lift increment is nearly independent of angle of attack and slightly non-linear with spoiler deflection. The lift increment decreases for large angles of attack, either positive (12°) or negative (−8°).

Shown in Figure 3.3 are the pitching-moment characteristics: for a constant angle of attack the pitching-moment increases as the spoiler deflection increases; for a fixed spoiler deflection, and for moderate angles of attack (0° to 8°), the pitching-moment is approximately constant; and at stall the pitching-moment decreases abruptly. Apparent at negative angles of attack is a change in the pitching-moment curve character with spoiler deflection: this change in character is due to the forward movement of the lower surface boundary layer separation point, from the airfoil trailing edge, as the spoiler deflection increases. The pitching-moment coefficient displays a slight variation between the two Reynolds numbers tested.

12

The pitching-moment increment (the pitching-moment change due to spoiler deflection) as a function of spoiler deflection is displayed in Figure 3.4 for the highest Reynolds number tested (5.2×10^5). For moderates angles of attack ($0°$ to $8°$) the pitching-moment increment is slightly non-linear with spoiler deflection and nearly independent of angle of attack. The pitching-moment increment increases for large positive angles of attack below stall and decreases for large negative angles of attack.

Spoiler deflection affects the pressure distribution over the airfoil surface for angles of attack below stall. With increasing spoiler deflection the features displayed are (see Figure 3.5):

- The pressure increases over the upper surface (ahead of the spoiler) and decreases over the lower surface.

- The flow separates in the region behind the spoiler and is denoted by nearly constant pressure (base pressure).

Figure 3.5 also illustrates that the pressure increase on the upper surface (ahead of the spoiler) is greater than the pressure decrease on the lower surface for a given spoiler deflection and positive angles of attack below stall. At negative angles of attack this pressure variation was not as clearly displayed. At angles of attack above stall ($> 16°$), spoiler deflection has no effect on the pressure distribution: flow separation occurs so far forward on the airfoil that the spoiler is in the "dead air" region of the resulting wake. With increasing spoiler deflection, the pressure at the spoiler hingeline tends towards stagnation ($Cp = +1.0$); however, this level is not reached due to thickening or separation of the boundary layer in that region.

The dependence of the base pressure coefficient on angle of attack and spoiler deflection is shown in Figure 3.6. For a constant angle of attack, the base pressure decreases with increasing spoiler deflection. A main feature of bluff body flows is that the base pressure is less than the free stream pressure. This negative pressure on the rear side of the body and the positive pressure on the forward side results in a net pressure drag, that is distinct from, and many times larger than the skin friction drag. The base pressure is indicative of the behavior of the pressure drag and approximately the total drag of the airfoil-spoiler configuration.

13

The lift, moment, and surface pressure characteristics found here agree with previous investigations into the aerodynamics of spoilers (see Mack et al. [8] and Wentz et al.[11]) and the analogous lift increasing counterparts to spoilers, split flaps (see Wenzinger et al.[24,25] and Wallace[26]).

3.2.2 Boundary Layer Survey

General Remarks

Velocity measurements in the boundary layer over the upper surface of the airfoil, ahead of the spoiler, were made at 0° angle of attack. They reveal that at large spoiler deflections the adverse pressure gradient ahead of the spoiler can cause the boundary layer to separate; also, the state of the boundary layer determines the onset of separation and the separation characteristics displayed. In these measurements two boundary layer types were encountered, turbulent and transitional, corresponding to Reynolds numbers of 5.2 and 2.8 $\times$ 10^5, respectively.

Re= 5.2 $\times$ 10^5 *(Turbulent Boundary Layer)*

At 0° angle of attack separation of the turbulent boundary layer occurred for a spoiler deflection of 60°. For spoiler deflections less than 60°, the turbulent boundary layer was able to negotiate the hingeline without separation. Boundary layer development over the upper surface of the airfoil is illustrated in the mean and turbulence intensity velocity profiles shown in Figure 3.7 for a spoiler deflection of 60°, only points inside the hot-wire calibration range are shown. Evident is the rapid thickening of the turbulent boundary layer upon approach to the spoiler hingeline. The boundary layer separates close to the hingeline ($x/c \sim .7$) and reattaches on the spoiler face (as indicated by measurements at the spoiler tip); forming a separation bubble at the spoiler hingeline.

Re= 2.8 $\times$ 10^5 *(Transitional Boundary Layer)*

Separation of the transitional boundary layer occurred for spoiler deflections of 60° and 30°, at 0° angle of attack; the characteristics displayed are typical of laminar separation bubbles as discussed by Bursnall et al.[27], Gault[28], and Chapman et

14

al.[29]. These characteristics are: One, the shape factor rapidly increases after separation and rapidly decreases upon the free shear layer transition to turbulence; Two, the surface pressure distribution displays a discontinuity, "kink", at the transition location. Figure 3.8 shows the shape factor as a function of chordwise position for a spoiler deflection of 60°; the turbulent boundary layer case (Re= 5.2 × 10^5) is included for comparison. For the spoiler deflection of 60° separation occurs farther forward ($x/c \sim .4$) on the airfoil than in the turbulent boundary layer case. It is not clear from the data if the separated shear layer reattaches ahead of the spoiler hingeline or on the spoiler face. The pressure distribution, at 0° angle of attack, is shown in Figure 3.9; the higher Reynolds number (Re= 5.2 × 10^5) case is included for comparison. Readily visible is the "kink" in the pressure distribution, associated with transition in the separated free shear layer at the lowest Reynolds number (Re= 2.8 × 10^5), for spoiler deflections of 60° and 30°. For both Reynolds numbers tested the boundary layer was able to negotiate the hingeline without separation at spoiler deflections of 15° and 0°; the pressure distributions at these spoiler deflections show no difference between the two Reynolds numbers tested.

3.2.3 Wake Mean Velocity Field

The turbulent wake generated by the deflected spoiler is highly unsteady and complex in nature. On the other hand, the time averaged flow field manifests a simpler structure — a region of reversed flow exists just behind the spoiler and closes downstream of the airfoil trailing edge. The closure distance increases with spoiler deflection. This structure of the near wake is displayed in the dual split film velocity vector plots shown in Figure 3.10 for spoiler deflections of 15°, 30°, and 60°. Also, features of the overall time averaged flow field are displayed in the velocity vector plots of Figure 3.11: illustrated is the increase in the wake width (the "bluffness" of the airfoil-spoiler configuration) with increasing spoiler deflection; the decrease in circulation with increasing spoiler deflection, evident by the negative flow angles forward of the airfoil; and the affect of spoiler deflection on the upper surface boundary layer development (only qualitatively correct due to probe interference — see section 2.5). As is evident the increasing "bluffness" of the configuration as the spoiler deflection increases results in a displacement in

15

the outer flow streamlines. It is this displacement of the outer flow streamlines that alters the surface pressure distribution and the resulting forces and moment resulting from the pressure distribution.

3.3 Unsteady Flow Field Characteristics

3.3.1 General Remarks

The unsteady nature of the flow field generated by an airfoil with deflected spoiler is of interest in view of the following: One, "buffet" of the horizontal tail and the wing itself through interaction with the spoiler generated turbulent wake; Two, the mean flow field, the determinant of the overall mean forces and moments, is itself determined by the "mixing" process of the unsteady flow field; Three, from consideration of item two it has been intimated (see Ayoub et al.[12]) that the non-linear control effectiveness of spoilers is due to changes in the character of the unsteady flow field as the spoiler is deflected.

Vortex shedding characterizes the turbulent wake generated by the deflected spoiler; and occurred for all the spoiler deflections (5° to 60°) and for both Reynolds numbers tested. Figure 3.12 displays the vortex shedding frequencies[3] encountered as a function of spoiler deflection. The frequency of the vortex shedding decreases as the spoiler deflection increases. This correlation agrees with the observations of Roshko[20,21] and Fage et al.[22,23] on bluff bodies: the vortex shedding frequency is inversely related to the width of the wake – "bluffness" – of the body.

The flow visualization of the vortex formation process shows that at large spoiler deflections the vortex shedding is extremely periodic and regular; however, as the spoiler deflection decreases the vortex shedding becomes less regular, more intermittent. This change in the vortex shedding character with spoiler deflection manifests itself in the fluctuating wake velocity and surface pressure signals as a narrowband character.

3.3.2 Wake Unsteady Velocity Field

The vortex shedding frequency shift is also illustrated in the wake power spectra of Figure 3.13; conditions in Figure 3.13 are 0° angle of attack and the lowest Reynolds number tested (Re= 2.8×10^5). The spectra are from a single hot-wire

---

[3]The vortex shedding frequency is defined as that due to passage of one side of the vortex street (see appendix E-2.2 for how f was determined).

17

at the lower edge of the wake, horizontally positioned .6 chords downstream of the airfoil trailing edge. The vertical position varied with spoiler deflection. Also, power spectra at various locations in the wake (obtained using the dual split film probe) show that the maximum amplitude of the energy "spike" associated with the vortex shedding decreases as the spoiler deflection decreases. From the wake power spectra (see Figure 3.13) it is evident that the vortex shedding displays narrowband characteristics: the vortex shedding energy concentrates in a frequency band; spoiler deflection determines the band width. At high spoiler deflections (e.g. 60°; see Figure 3.13) the band is narrow; with decreasing spoiler deflection (e.g. 5°; see Figure 3.13) the band widens. This narrowband character of the vortex shedding is obvious in the autocorrelation function of the wake velocity signal. The wake autocorrelation is shown in Figure 3.14 along with the wake power spectra and wake velocity signal for two spoiler deflections (60° and 5°); the autocorrelation, spectra, and signal are from the same single hot-wire used for the wake power spectra of Figure 3.13.

The geometry of the airfoil with deflected spoiler is analogous to simply shaped bluff bodies. Comparison of the shedding frequency characteristics of the spoiler to the shedding frequency of other bluff bodies is best done in non-dimensional form. The appropriate characteristic length to form a Strouhal number is the spoiler projection height above the airfoil trailing edge. Plotted in Figure 3.15 is the Strouhal number $(S_{,h})$ as a function of spoiler deflection for 0° angle of attack (the data is blockage corrected). Depending on the spoiler deflection, the Strouhal number agrees with those of simply shaped bluff bodies:[4] a circular cylinder for spoiler deflections less than 30°; a 90° wedge at a spoiler deflection of approximately 55° ; and a normal plate when the data is linearly extrapolated to a spoiler deflection of approximately 95°. The simply shaped bluff body Strouhal number values are those corresponding to a Reynolds number range based on the spoiler projection height.

Also shown in Figure 3.15 for comparison are the results of Wentz et al.[11] for a similar airfoil (identical airfoil sections; spoiler chords differ, Wentz .157c,

---

[4]Bluff body Strouhal number values are from Roshko[20]

present test .1554c) at a Reynolds number of 2.2×10^6. Agreement with the present test is dependent on spoiler deflection: poor at low spoiler deflections, but improving at large spoiler deflections. This comparison suggests that the Strouhal number depends on Reynolds number, and that this dependence decreases at large spoiler deflections. Intuition supports this, since at large spoiler deflections the abrupt changes the separating boundary layer goes through, at the spoiler tip, should negate any influence of upstream boundary layer development on the wake characteristics. Slight dependency of the present test values on Reynolds number is shown, supporting this hypothesis. This dependence is a maximum at low spoiler deflections (15° and 20°) and decreases with increasing spoiler deflection; there is negligible dependence at a spoiler deflection of 60°. However, care must be exercised in drawing conclusions from the present test, since the Reynolds number range is limited.

Of note is that the Strouhal number results for Wentz et al.[11] also show agreement with the value for a normal plate when linearly extrapolated to a spoiler deflection of approximately 95° (see Figure 3.15).

The Reynolds number dependence of the Strouhal number manifests itself more clearly in Figure 3.16: where the Strouhal number (S_h) is plotted as a function of Reynolds number (Re_h) for 0° angle of attack (the data is blockage corrected); both numbers are based on the characteristic length h, the spoiler projection height. The results of Wentz et al.[11] are included for comparison. For a constant spoiler deflection the Strouhal number increases with Reynolds number; this change in the Strouhal number, as a function of the Reynolds number, increases with decreasing spoiler deflection. This is shown by the present results and those of Wentz et al.[11].

In the nomenclature of wind tunnel testing the variation of the non-dimensional coefficients with Reynolds number is referred to as "scale effect": according to Dryden[30] — "scale effect, - - - , can be adequately understood only in terms of knowledge of the state of flow in the boundary layer". The author believes that the Reynolds number dependence ("scale effect") of the Strouhal number in the present test (and in comparison to the results of Wentz et al.[11]) is due to changes in the character of the boundary layer flow; this conclusion is supported by the present

19

test boundary layer survey results (see section 3.2.2).

From the bluff body investigations of Roshko[20,21] it is known that the base pressure and the overall flow field of a bluff body is critically determined by the dynamics of the vortex formation just downstream of the body. Motivated by this work the relationship between the shedding frequency and the base pressure is plotted in non-dimensional form ($S_{,c} - vs - Cpb$), in Figure 3.17. For a constant spoiler deflection the shedding frequency decreases with increasing base pressure. This correlation, for a constant configuration shape, agrees with the observations of Roshko[20,21] on bluff bodies. At a constant angle of attack the shedding frequency and base pressure decrease with increasing spoiler deflection.

3.3.3 Fluctuating Surface Pressure

The vortex shedding induces a fluctuating pressure field over the surface of the airfoil. A typical example of the level and frequency content of the surface pressure fluctuations is illustrated in Figure 3.18: presented are surface pressure power spectra for a spoiler deflection of 60°, 0° angle of attack, and the highest Reynolds number tested (5.2×10^5). For this representative example the vortex shedding frequency is 215.0 Hz; readily apparent in the power spectra at that frequency is the energy "spike" associated with the vortex shedding. Of note is that this energy "spike" is discernible over the entire airfoil surface. Also, near the trailing edge region an energy "spike" is perceptible in the power spectra at twice the vortex shedding frequency: due to the proximity of the vortex formation region both the upper and lower rows of the vortex street are sensed. Apparent in some of the surface pressure power spectra is a "spike", at a frequency of 60 Hz, associated with an instrumentation ground loop.

The effect of spoiler deflection on the fluctuating surface pressure characteristics is exhibited in the pressure power spectra of Figure 3.19; conditions in Figure 3.19 are 0° angle of attack and the highest Reynolds number tested (5.2×10^5). The spectra are from the unsteady pressure transducer located at the airfoil lower surface trailing edge; for clarity only that part of the spectra containing the energy "spike" associated with the vortex shedding frequency is displayed. As expected, since both

20

are induced by the vortex shedding, the surface pressure power spectra display the same characteristics as the wake velocity power spectra: namely, a narrowband character; the bandwidth decreases as the spoiler deflection increases; and the maximum amplitude of the energy "spike" associated with the vortex shedding frequency decreases as the spoiler deflection decreases.

Exhibited in Figure 3.20 is the chordwise distribution of the RMS peak value of the pressure spectra "spike" associated with the vortex shedding frequency for three spoiler deflections (60°, 30°, and 15°). The RMS surface pressure level (f component) is a maximum at the airfoil lower surface trailing edge region and decreases one order of magnitude going towards the airfoil leading edge; and increases as the spoiler deflection increases. In order to appreciate the magnitude of the fluctuating surface pressure field the RMS surface pressure level is normalized with respect to the free stream dynamic pressure. Of note, is the magnitude of the normalized RMS surface pressure level at the airfoil lower surface trailing edge region: it ranges from approximately .06 to .01, these values translate into absolute RMS surface pressure levels of 6% to 1% of the free stream dynamic pressure, corresponding to spoiler deflections of 60° to 15°, respectively.

Shown in Figure 3.21 is the RMS surface pressure level associated with the vortex shedding frequency, at each chordwise measurement location, plotted as a function of spoiler deflection; the RMS surface pressure level is normalized with respect to the free stream dynamic pressure. In general, at a specific chordwise location, the change in the RMS surface pressure level, as the spoiler deflection increases, is dependent on the spoiler deflection: it changes rapidly at low spoiler deflections (0° to 30°); and changes little, being approximately constant at some measurement locations, at high spoiler deflections (30° to 60°). As is shown in Figure 3.22, this same characteristic is displayed by the RMS surface pressure level associated with twice the vortex shedding frequency.

3.3.4 Flow Visualization of the Near Wake Structure

The formation of vortices characterizes the near wake structure of the airfoil-spoiler configuration. The vortices are formed through the interaction of the two

free shear layers that arise from separation of the boundary layers at the spoiler tip and the airfoil trailing edge. These two free shear layers are unstable, the instability manifests itself in the tendency of the shear layers to roll-up alternately into discrete vortices near the airfoil trailing edge. This formation of vortices in the spoiler wake occurs in the same manner as the formation of the vortex street in the wake of a circular cylinder.

The vortex formation process is shown in the schlieren photographs of Figure 3.23, for 0° angle of attack, and three spoiler deflections (60°, 30°, and 15°). For each spoiler deflection a sequence of photographs shows the vortex formation process at selected instants in time[5] throughout one vortex shedding shedding cycle. The viewing area is the airfoil trailing edge region ($x/c \approx .65$ to 1.35). The schlieren knife edge is vertical. Further discussion of the schlieren method[6] used is given in Appendix D. The shear layer roll-up into vortices is easier to discern in the photographic sequence for a spoiler deflection of 60°, Figure 3.23a. The shear layers are visible as regions of contrast. The airfoil trailing edge region, where the shear layer interaction and roll-up occurs, is approximately in the center of the viewing area. The region of free shear layer interaction and "roll up" is referred to by Roshko[20,21] as the "coupling region".

Schlieren movies of the vortex formation process were also made. Visual observation of these movies revealed that the regularity of the vortex formation process depends on spoiler deflection. As the shear layers are brought closer together, i.e., as the spoiler deflection decreases, the regularity of the vortex formation process breaks down and the vortex shedding becomes intermittent. At large spoiler deflections the vortex shedding is regular and periodic. This correlates with the narrowband characteristic displayed by the fluctuating velocity and surface pressure measurements.

---

[5]The time is displayed under each photographic frame as a phase angle increment of the vortex shedding period. Note, that frames $\phi = 0°$ and 360°, for each spoiler deflection photographic sequence, taken at different times, indicate exactly the same flow pattern.

[6]To use the schlieren method the airfoil surface was heated to artificially enhance the refractive index of the flow; therefore, only the global features displayed provide an indication of the nature of the flow.

IV. CONCLUSIONS and RECOMMENDATIONS

4.1 Conclusions

A summary of the results of the experimental study described in this dissertation follows.

Steady Flow Field

- The lift, moment, and surface pressure characteristics found agree with those of previous investigations into spoilers and the analogous lift increasing counterparts of spoilers, split flaps.

- Separation of the boundary layer, ahead of the spoiler, for large spoiler deflections, depends on the boundary layer character. A turbulent boundary layer forms a separation bubble at the spoiler hingeline; a transitional boundary layer separates further forward and displays characteristics typical of laminar separation bubbles.

- The wake mean velocity field is characterized by a closed region of reversed flow just aft of the spoiler; the closure distance increases with spoiler deflection.

Unsteady Flow Field

- The unsteady nature of the wake is characterized by vortex shedding over a wide range of angle of attack, spoiler deflection, and Reynolds number, the displayed vortex shedding characteristics are in agreement with those of simply shaped bluff bodies, and are typical of bluff bodies in general.

- The regularity of the vortex shedding is dependent on the spoiler deflection: namely, the vortex shedding displays narrowband characteristics (as manifested in the wake velocity fluctuations and the surface pressure fluctuations); the bandwidth being dependent on the spoiler deflection; the bandwidth decreasing as the spoiler deflection increases.

- The Strouhal number is dependent on the Reynolds number; this dependence raises a practical question: How does one extrapolate the vortex shedding frequency from low Reynolds number tests to full scale flight Reynolds numbers (approximately 20 to 40 $\times 10^6$, based on airfoil chord)?

- The RMS level of the fluctuating surface pressure field, associated with the vortex shedding frequency and twice the vortex shedding frequency, increases as the spoiler deflection increases.

- The vortex shedding frequency component of the fluctuating surface pressure field is of appreciable magnitude at large spoiler deflections.

Final Note

The flow past an airfoil with a deflected spoiler is only a specific problem within the area of bluff body aerodynamics. As pointed out earlier, it is known from bluff body aerodynamic studies that the near wake structure is the essential determinant of the outer flow and therefore the pressure distribution over the body. Furthermore, the vortex formation process determines the near wake structure. With these points in mind, two of the present studies findings are therefore noteworthy: first, that the vortex shedding regularity depends on the spoiler deflection; second, that the magnitude of the fluctuating surface pressure field associated with the vortex shedding depends on the spoiler deflection, and is of appreciable magnitude at large spoiler deflections. Though not conclusive, these findings do provide support to the speculation of Ayoub et al.[12] that the underlying cause of spoiler non-linear control effectiveness is a change in character of the unsteady flow field as the spoiler is deflected.

4.2 Recommendations for Future Research

As stated in the introduction the present study was exploratory in nature; more work remains to be done to gain a clear understanding of the aerodynamic features of spoiler flight controls. Unanswered questions that provide a departure for new work are: How do Reynolds number, Mach number (compressibility), and three dimensional affects – such as finite spoiler panel aspect ratio and wing sweepback – affect the flow field structure? What affect does flap deflection have on the flow

field structure? Is the speculation of Ayoub et al. – that spoiler non-linear control characteristics are linked to changes in the unsteady flow field – correct?

To the author a specific area that demands attention is the Reynolds number dependence ("scale effect") displayed by the Strouhal number in the present test: How does one extrapolate the vortex shedding frequency – or for that matter any of the unsteady flow field parameters – from low Reynolds number tests to full scale flight Reynolds numbers (approximately 20 to 40×10^6 based on airfoil chord)? This question needs to be addressed if test results are to be of use in the design engineering process. Therefore, it would be extremely informative to conduct a systematic series of tests on one configuration at various Reynolds numbers, from low to flight values, to gain an understanding of "scale effect".

Appendix A
Test section and Traversing Mechanism

An overall view of the test section and traversing mechanism used for the experiment is shown in Figure A-1.

The test section is 18 inches (45.72 cm) square by 35.5 inches (90.17 cm) long with an aluminum framework; circular turntables for model mounting and an access port are built into the detachable plexiglas sidewalls. When installed the test section vents to atmospheric pressure through a gap at its downstream end.

Bolted atop the test section the traversing mechanism provides translational motion along three orthogonal axes. Attachment of the steel tube probe (e.g. hot-wire, dual split film) support is to a block on the vertical axis slide. Probe support insertion into the test section is through a centerline longitudinal slot and multiple transverse slots in the top plate. The traversing mechanism is made from Velmex Corporation motor driven slide assemblies and support brackets: analog motors drive the two horizontal axes lead screws; a stepper motor drives the vertical axis lead screw. Control of the vertical axis lead screw, in continuous motion or selected incremental steps (minimum step size: .0005 inch/step), is provided by a Superior Electric stepper motor indexer (SP-153A). A Velmex analog controller provides continuous motion control of the two horizontal axes lead screws.

No backlash was detectable in the vertical axis lead screw assembly: however, probe data gathering traverses were only made in one direction to eliminate the possibility of backlash position error. Probe positioning along the horizontal axis was performed visually using the analog controller. A short range telescope was used to accurately position the probe at a known reference before movement.

Also, a centerline longitudinal slot is provided in the bottom plate of the test section for probe insertion. The probe support tube is mounted in a block, constrained to slide over the bottom of the plate by two rails. A clamp is used to fix the probe position.

26
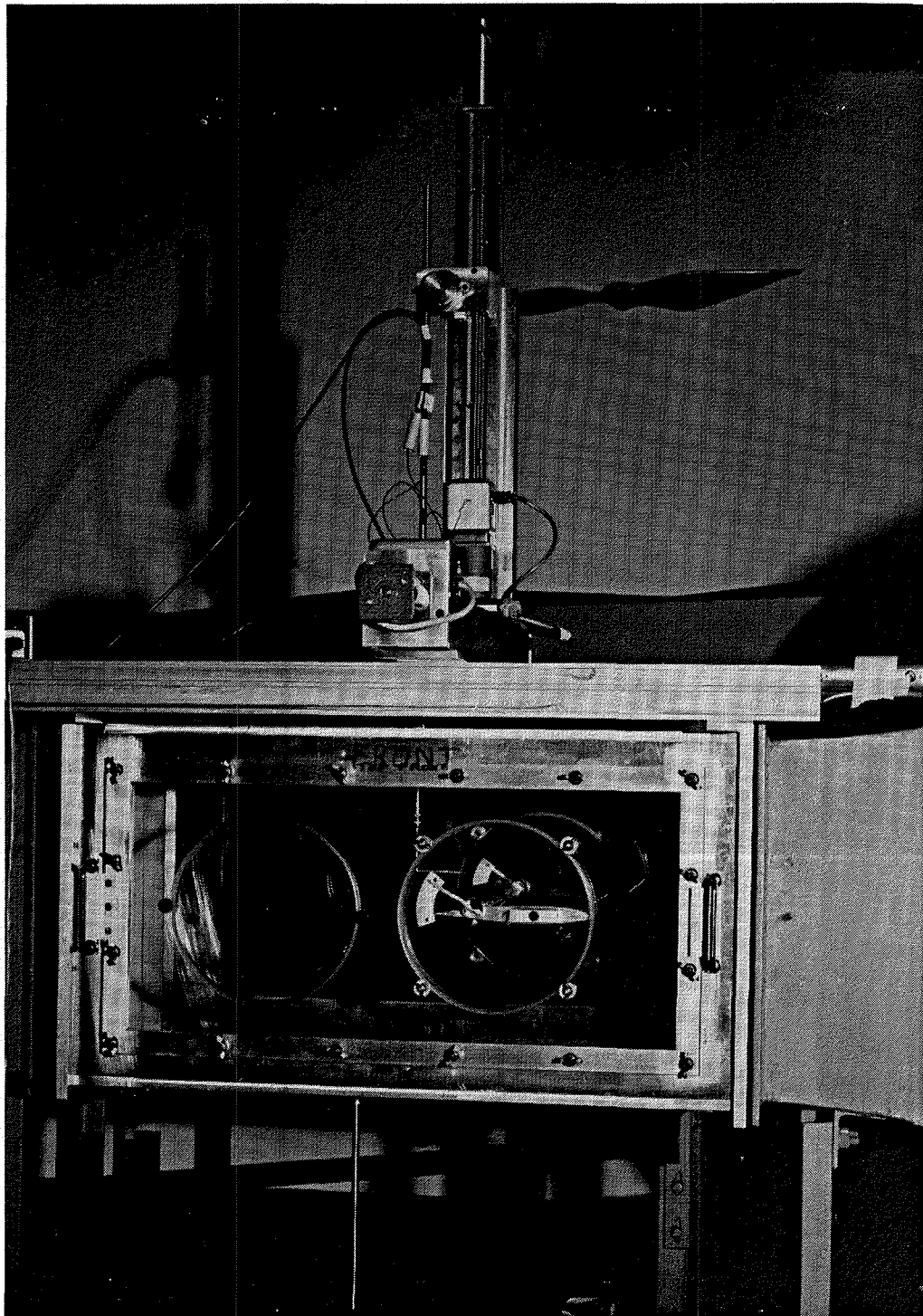
Figure A-1   Test section and traversing mechanism.

Appendix B
Model(s)– Construction and Mounting

Parameters and coordinates of the airfoil section tested are given in Table B-1.

Three aluminum two-dimensional models were used for the tests, each dedicated to a particular measurement.

Model No. 1: Velocity measurements in the airfoil surface shear layers and wake, and schlieren flow visualization of the near wake.

Model No. 2: Static surface pressure measurements.

Model No. 3: Fluctuating surface pressure measurements.

Reference may be made to Appendix D for details of the model instrumentation (e.g. transducer locations).

An overall view of the models is displayed in Figure B-1. Model no. 1 is composed of two pieces, airfoil-spoiler; models 2 and 3 were made with a deployable flap and are composed of three pieces, airfoil-spoiler-flap. However, all of the tests were performed with the flap in the stowed position (flap up – cruise configuration): models 2 and 3 being identical to model no. 1 in section for the tests.

For all three models two spoiler hinges were located four inches either side of midspan ($y = \pm 4$ in) to provide structural support and deflection of the spoiler about the hingeline axis. Also at the same spanwise locations, for models 2 and 3, two brackets were mounted on the lower surface to provide structural rigidity for the flap.

For the tests the models were horizontally mounted spanning the test section (see Figure B-2). The airfoil and spoiler pieces being mounted in individual circular turntables to facilitate angle of attack and spoiler deflection changes. During testing the spoiler hingeline was sealed with tape; on models 2 and 3 the flap cove (the discontinuity between the main airfoil body and flap) was covered with tape to present a smooth contour to the flow. Also, during testing the rigidity of the

28

deflected spoiler was checked using a short range telescope; no vibrations were detectable.

Table B-1

Airfoil Section Geometry

Station		Upper Surface		Lower Surface	
X (in.)	$\frac{X}{C}$	Z (in.)	$\frac{Z}{C}$	Z (in.)	$\frac{Z}{C}$
0	0	0	0	0	0
.0040	.0005	.0296	.0037	-.0144	-.0018
.0080	.0010	.0400	.0050	-.0216	-.0027
.0200	.0025	.0624	.0078	-.0344	-.0043
.0400	.0050	.0896	.0112	-.0464	-.0058
.1200	.0150	.1656	.0207	-.0784	-.0098
.1600	.0200	.1936	.0242	-.0896	-.0112
.2000	.0250	.2168	.0271	-.1000	-.0125
.3000	.0375	.2672	.0334	-.1216	-.0152
.4000	.0500	.3072	.0384	-.1400	-.0175
.6000	.0750	.3720	.0465	-.1728	-.0216
.8000	.1000	.4168	.0521	-.2032	-.0254
1.0000	.1250	.4528	.0566	-.2304	-.0288
1.2000	.1500	.4792	.0599	-.2560	-.0320
1.6000	.2000	.5144	.0643	-.3000	-.0375
2.0000	.2500	.5320	.0665	-.3336	-.0417
2.4000	.3000	.5392	.0674	-.3560	-.0445
2.8000	.3500	.5384	.0673	-.3664	-.0458
3.2000	.4000	.5336	.0667	-.3656	-.0457
3.6000	.4500	.5232	.0654	-.3544	-.0443
4.0000	.5000	.5088	.0636	-.3336	-.0417
4.4000	.5500	.4904	.0613	-.3064	-.0383
4.8000	.6000	.4680	.0585	-.2752	-.0344
5.2000	.6500	.4384	.0548	-.2424	-.0303
5.6000	.7000	.4024	.0503	-.2080	-.0260
6.0000	.7500	.3600	.0450	-.1744	-.0218
6.4000	.8000	.3072	.0384	-.1392	-.0174
6.8000	.8500	.2456	.0307	-.1056	-.0132
7.2000	.9000	.1744	.0218	-.0720	-.0090
7.6000	.9500	.0928	.0116	-.0376	-.0047
8.0000	1.0000	.0032	.0004	-.0032	-.0004

Airfoil Chord (C)   - 8 in. (0.2032 m)
Maximum Thickness - 0.113C
Spoiler Chord   - 0.1554C
Spoiler Hingeline - 0.733C
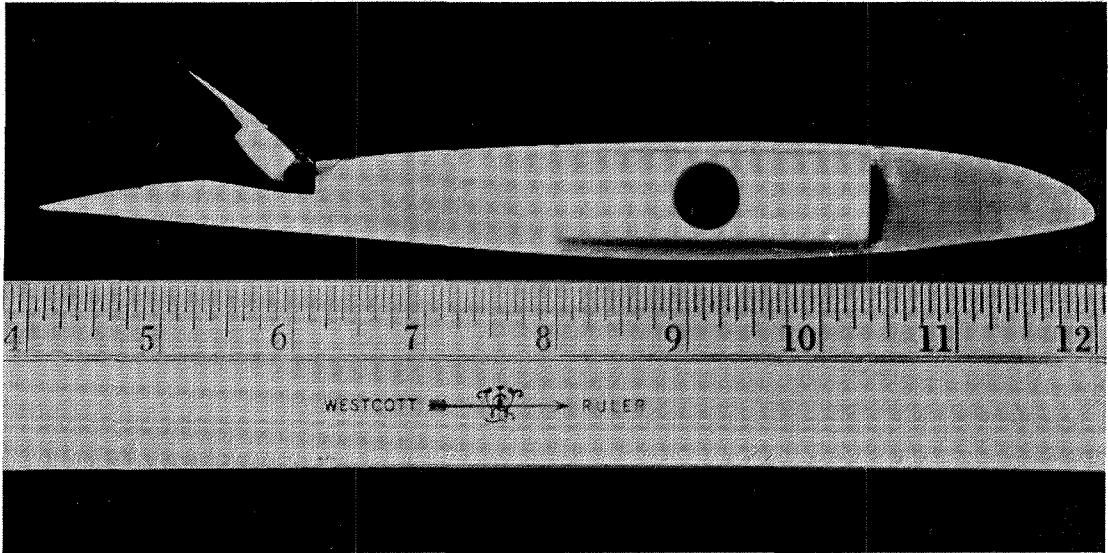
Model 1
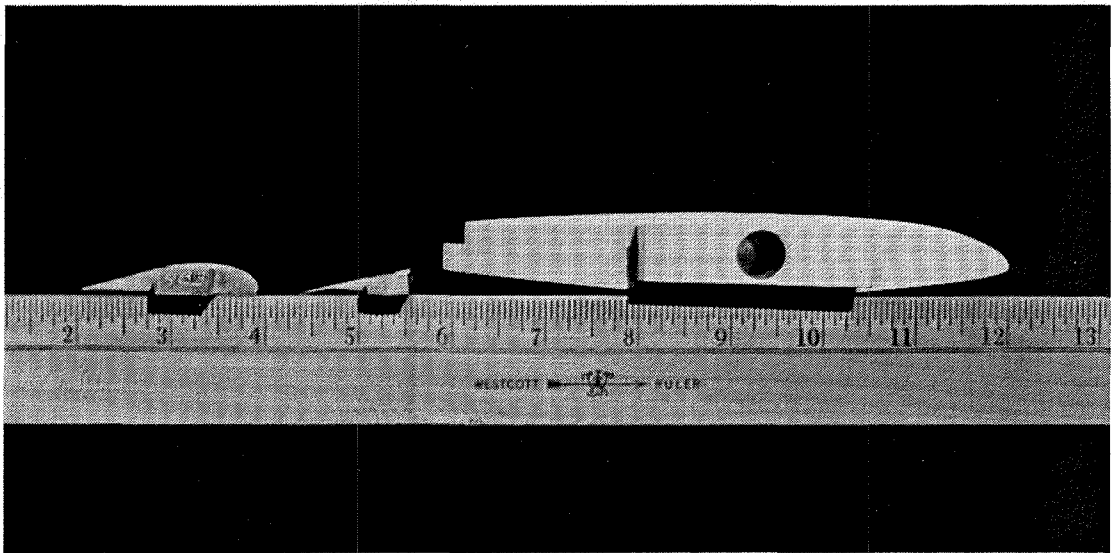
Model(s) 2 and 3

Figure B-1 Section view of model(s).

31
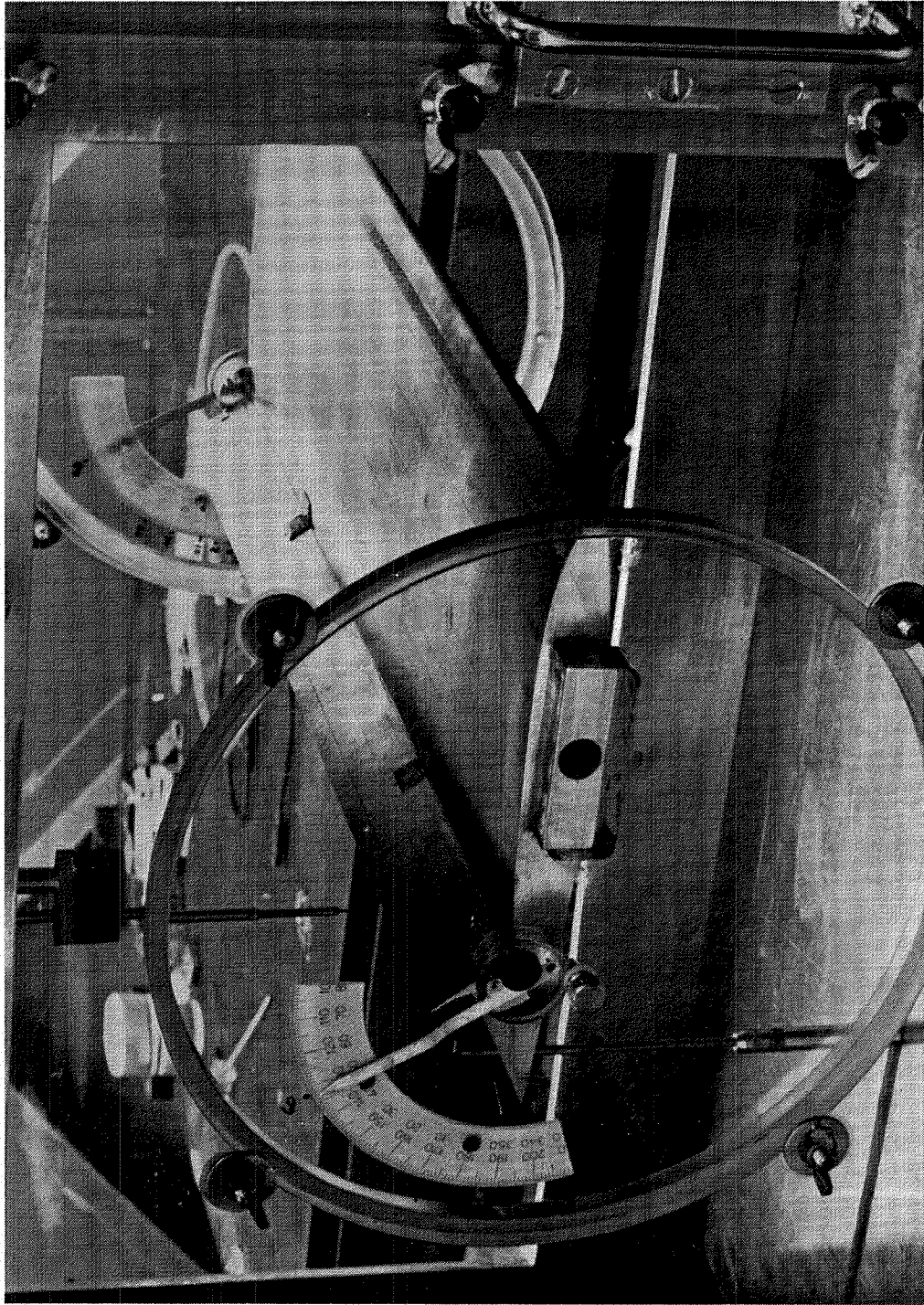
Figure B-2 Model in test section - view through side window.
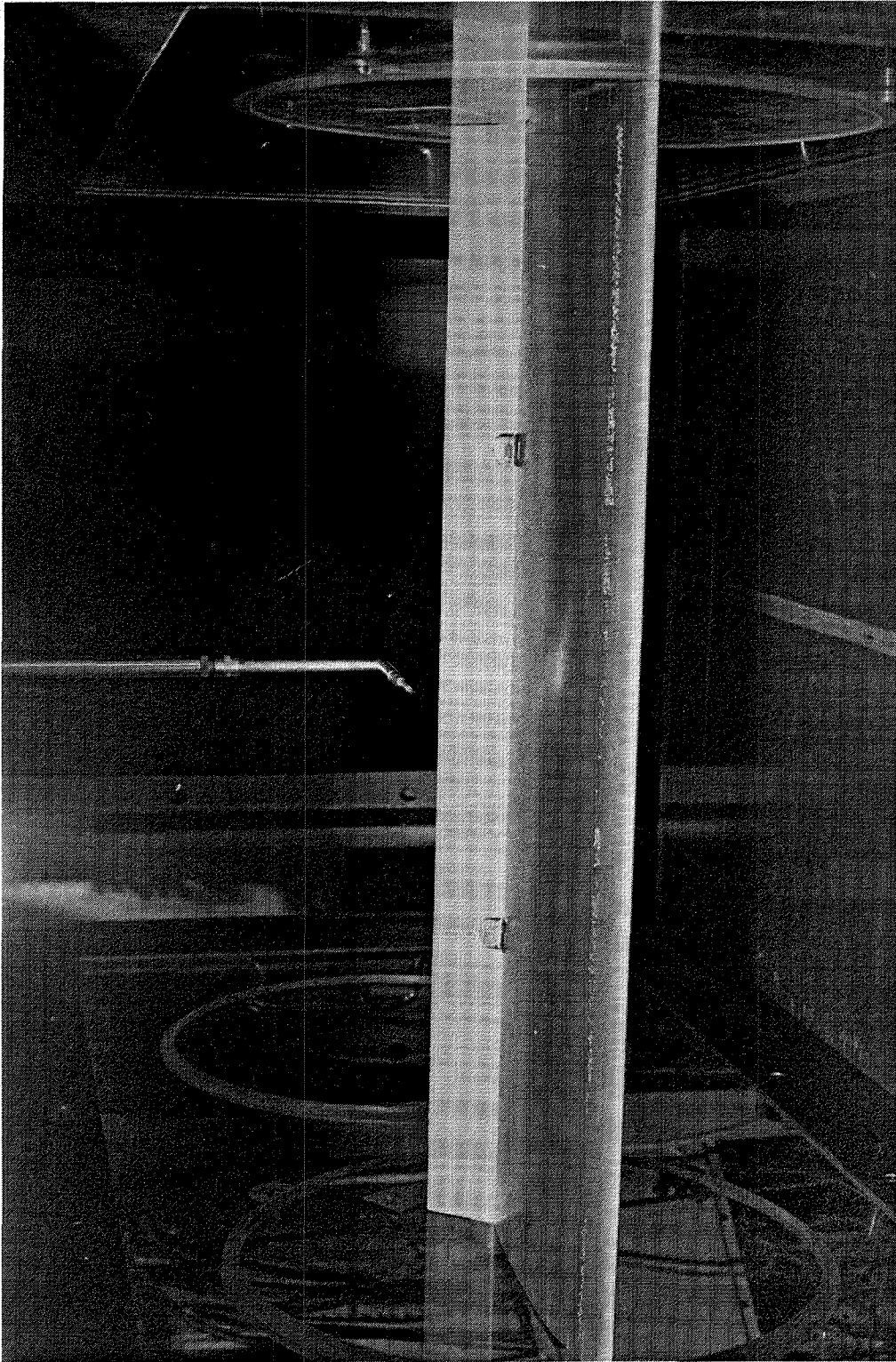
Figure B-2 (continued) Model in test section – view looking downstream.

Appendix C
Two-Dimensionality of Flow over Model(s)

Two-dimensionality of the flow over the model was indicated for angles of attack below stall by the following (see Figure C-1):

- Agreement of the chordwise static surface pressure distributions from the three spanwise locations $(2y/b = 0, \pm 1/3)$.

- Uniformity of the spanwise static surface pressure distribution $(x/c = .3)$.

Spanwise uniformity of the surface static pressure field is a necessary, but not sufficient, condition for two-dimensionality of the flow. As a further check for flow two-dimensionality surface flow visualization was performed, using kerosene as the surface pattern indicator. Visual inspection of the surface flow pattern, at various spoiler deflections with the wind tunnel running, indicated two-dimensionality of the surface flow over the model.
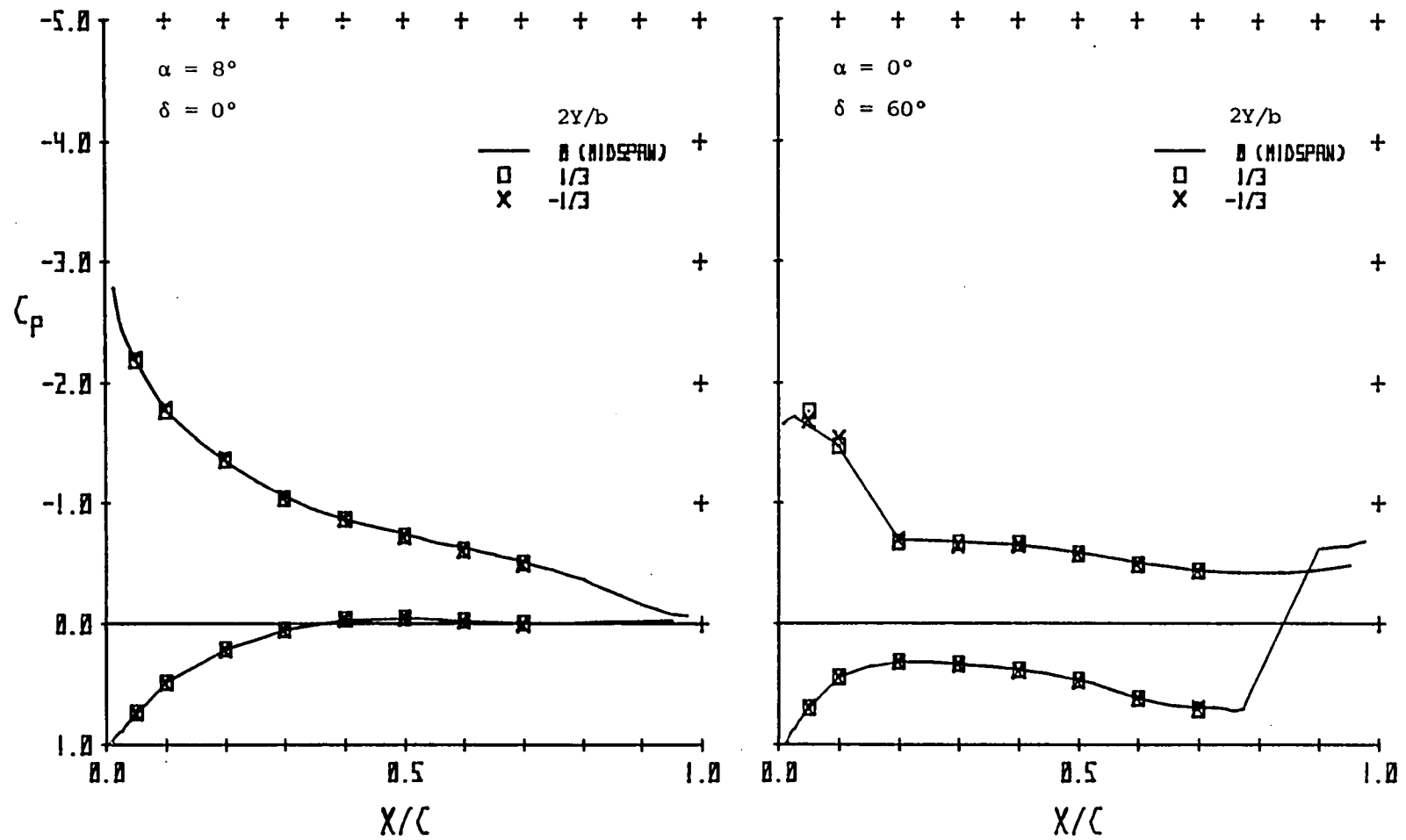
Figure C-1a   Representative comparisons of the three chordwise static surface pressure distributions for angles of attack below stall: Re = 5.2 x 10^5.
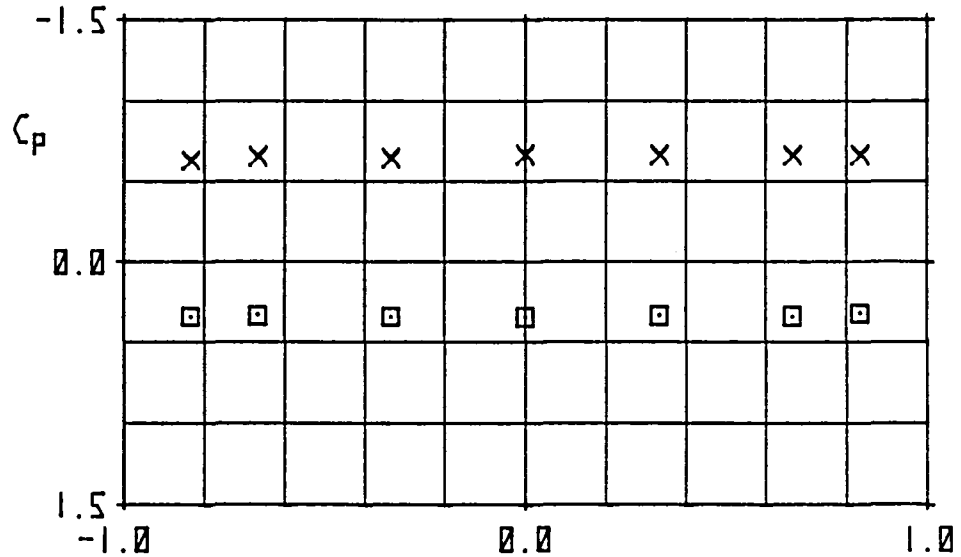
Figure C-1b   Representative spanwise static surface pressure
distributions for angles of attack below stall.

36

Appendix D

Instrumentation – Details

The data acquisition systems and the model(s) instrumentation are described in this section. The outline of presentation is as follows:

D-1 Static Surface Pressure

D-2 Boundary Layer Velocity Survey (hot-wire anemometry)

D-3 Wake Velocity Survey (dual split film anemometry)

D-4 Fluctuating Surface Pressure

D-5 Flow Visualization

D-1 Static Surface Pressure

The locations of the static pressure holes distributed over the surface of model no. 2 are given in Table D-1.

Displayed in Figure D-1 is a block diagram of the static pressure data acquisition system. A conventional Scanivalve system (four type 'J' 24 port units) was used to measure the static pressure. The Scanivalve pressure transducer (Gould, range ± 5 p.s.i.d.) signals, after passing through signal conditioners (B&F model 1-700SG), were amplified (NEFF type 126) and sent to the analog/digital interface of a micro-computer (HP-9830A) for analysis.

The scanivalve pressure transducers were statically calibrated; each calibration curve was found to be linear.

D-2 Boundary Layer Velocity Survey (hot-wire anemometry)

Shown in Figure D-2 is a block diagram for the boundary layer velocity survey instrumentation set-up. Two single channel hot-wire anemometers with linearizers (DISA 'M' series) were used. One hot-wire probe (DISA type P-15; 5μm dia.) was

traversed through the boundary layer, in a vertical path, i.e., normal to the airfoil mean chord line, at the airfoil midspan. The other hot-wire probe (DISA type P-14; 5μm dia) was used to provide a velocity signal of the vortex shedding and was located at the lower edge of the wake: .6 chords downstream of the airfoil trailing edge, the vertical position varied with spoiler deflection. Both hot-wires were horizontally aligned normal to the flow. The linearized boundary layer hot-wire signal was input to the analog/digital interface of a micro-computer (HP-9830A) for processing (mean and r.m.s. velocity) and storage on digital tape. Also, at selected flow field locations the a.c. component of both linearized hot-wire signals, after passing through amplifiers (NEFF type 126), were recorded on a 14 channel FM recorder (Sangamo 3500) for off-line time series analysis.

The hot-wire probes were calibrated using a DISA hot-wire calibrator; being linearized over velocity ranges of 50-10 m/s and 25-5 m/s, corresponding to the two test Reynolds numbers of 5.2 and 2.8×10^5, respectively.

D-3 Wake Velocity Survey (dual split film anemometry)

The dual split film data acquisition system was developed by the Boeing Company; the details of which are proprietary. In general the system is similar to the hot-wire boundary layer velocity survey data acquisition system: the anemometer signals being interfaced with a micro-computer for processing, and the a.c. component of the signals being recorded on an FM tape recorder for off-line time series data analysis. A dual split film probe (TSI model 1288BJ), aligned horizontally normal to the flow, was used to measure the mean velocity, mean flow angle, and two turbulence components in the vertical (x-z) plane. This probe consists of a quartz rod (.006 in. dia., .120 in. long), with a platinum film sensing area, mounted between two sting supports. Calibration of the dual split film probe was performed in an air jet produced by a Boeing Company designed calibrator.

For a general description of split film anemometry reference may be made to Olin et al..

References

Olin, J.G., and Kiland, R.B., "Split-Film Anemometer Sensors for Three-

Dimensional Velocity-Vector Measurement," Proceedings of Symposium on Aircraft Wake Turbulence, Seattle, Washington, September 1970, Plenum Press, New York, 1971.

D-4 Fluctuating Surface Pressure

Table D-2 provides the locations of the eleven unsteady pressure transducers (Kulite model LQ-125-10) distributed over the surface of model no. 3.

A block diagram of the fluctuating surface pressure data acquisition system is shown in Figure D-3: the transducer signals were passed through signal conditioners (B&F model 1-700SG), amplified (NEFF type 126), and d.c. blocked (since only the a.c. component was of interest) before recording on a 14 channel FM tape recorder (Sangamo 3500) for later time series analysis. Also, a single channel hot-wire anemometer with linearizer (DISA 'M' series) was employed to provide a velocity signal of the vortex shedding, to be used as a reference (e.g. cross-correlations). The hot-wire probe (DISA type P-14, 5μm dia.), horizontally aligned normal to the flow, was located at the wake lower edge: .6 chords downstream of the airfoil trailing edge, the vertical position varied with spoiler deflection. For later time series analysis the a.c. component of this reference hot-wire signal was recorded on the FM tape recorder.

The unsteady pressure transducers were statically calibrated: each transducer calibration curve was found to be linear.

D-5 Flow Visualization

Unsteady flow visualization of the near wake structure was performed using the phase locked schlieren technique - described by Kadlec et al.

The schlieren set-up is shown in schematic form in Figure D-4. Optical glass ports were fitted into the test section sidewalls to provide viewing of the airfoil trailing edge region. Density gradients in the flow were artificially enhanced by heating four nichrome wires buried spanwise in the airfoil trailing edge region (see Table D-3). To provide a signal of the periodic velocity fluctuations induced by the

39

vortex shedding a single hot-wire probe was positioned at the wake lower edge. The hot-wire signal, with a phase locking device, was used to strobe the schlieren light source at a selected phase (i.e. time delay) in one period of the vortex shedding, the image of the flow field then being recorded on camera. In the phase locked schlieren photographs of Figure 3.23 the knife edge is horizontal.

A high speed movie (10^4 frames per second) was made of the vortex shedding process using the schlieren system in conventional fashion – the schlieren light source being on continuously.

References

Kadlec, R.A., and Davis, S.S., "Visualization of Quasiperiodic Flows," AIAA Journal, Vol. 17, No. 11, November 1979.

Static Pressure Hole Locations

Chordwise Distributions

Midspan		2Y/b = ±1/3	
X/C		X/C	
Upper Surface	Lower Surface	Upper Surface	Lower Surface
.0150	.0090	.0500	.0500
.0250	.0250	.1000	.1000
.0500	.1000	.2000	.2000
.0750	.2000	.3000	.3000
.1000	.3000	.4000	.4000
.1500	.4000	.5000	.5000
.2000	.5000	.6000	.6000
.2500	.6000	.7000	.7000
.3000	.7000		
.3500	.7500		
.4000	.8000		
.4500	.8500		
.5000	.9000		
.5250	.9500		
.5500			
.5750			
.6000			
.6250			
.6500			
.6750			
.7000			
.7250			
sp..7500			
sp..7750			
sp..8000			
.9000			
.9250			
.9500			
.9750			

Spanwise Distribution

X/C = .3	
±2Y/b	
Upper Surface	Lower Surface
.6667	.6667
.8333	.8333

Note:

1. b, model span = 18 in. (45.72 cm)

2. 'sp.' – Denotes the static pressure holes on the spoiler.

3. A static pressure hole is located on the aft face of the spoiler.

4. Hole diameter = .015 in. (.381 mm)
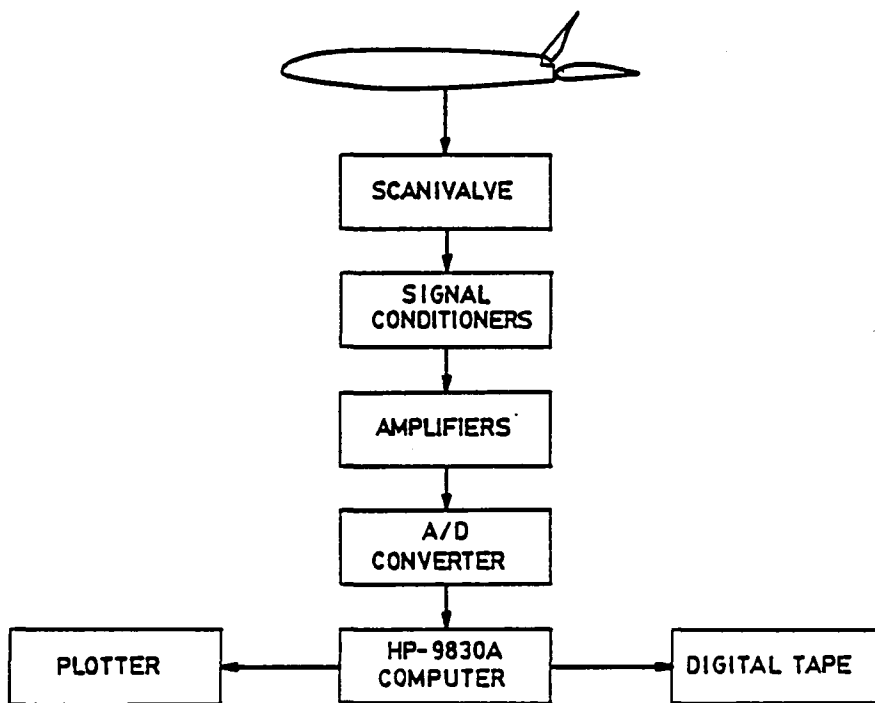
Figure D-1 Block diagram of static pressure measurement
system.
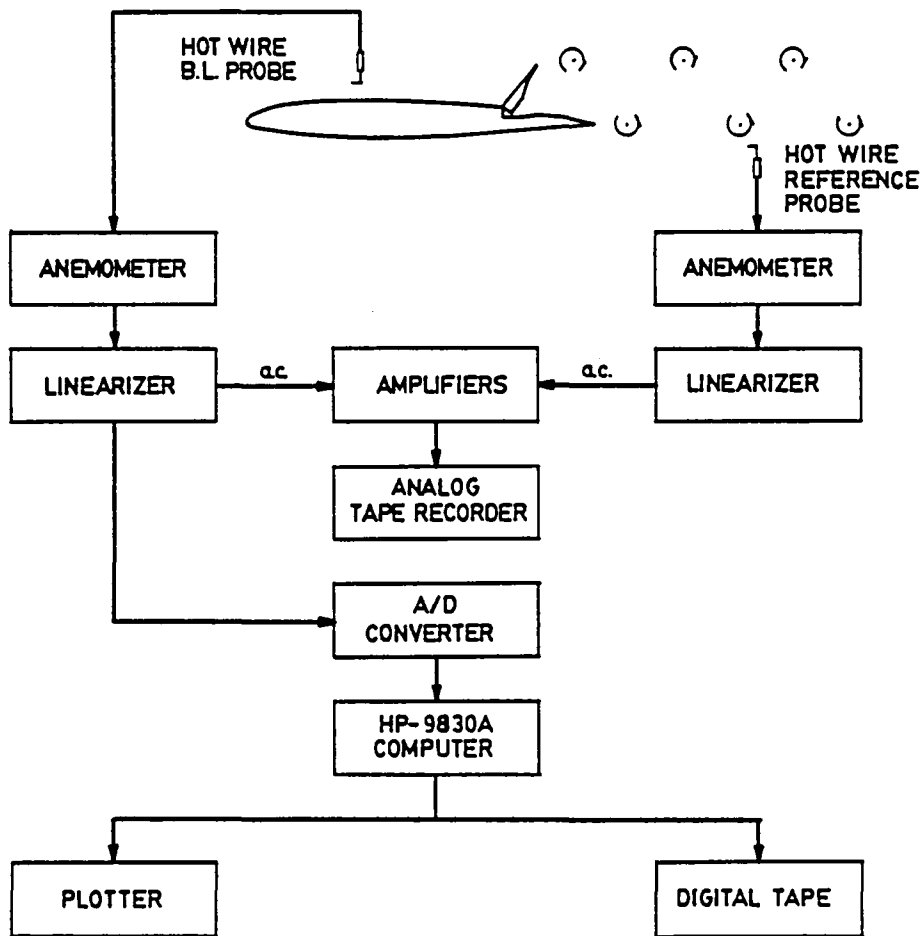
Figure D-2 Block diagram of boundary layer velocity
survey system.

Table D-2

Unsteady Pressure Transducer Locations
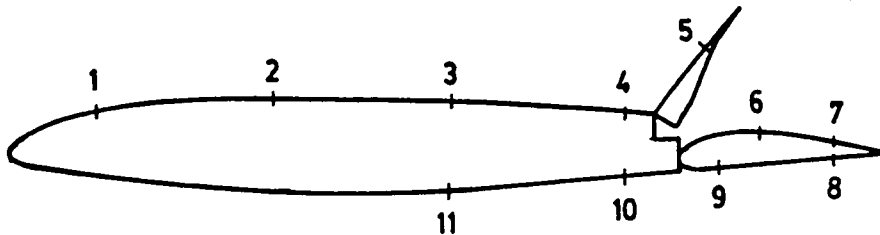
Chordwise Locations

Transducer No.	$\dfrac{X}{C}$
1	.100
2	.300
3	.500
4	.700
sp. 5	.825
6	.850
7	.950
8	.950
9	.800
10	.700
11	.500

NOTE:

1. The transducers are distributed midspan chordwise.

2. The transducer sensing area is flush with the airfoil surface.

3. 'sp.' - Denotes the transducer on the spoiler.

44
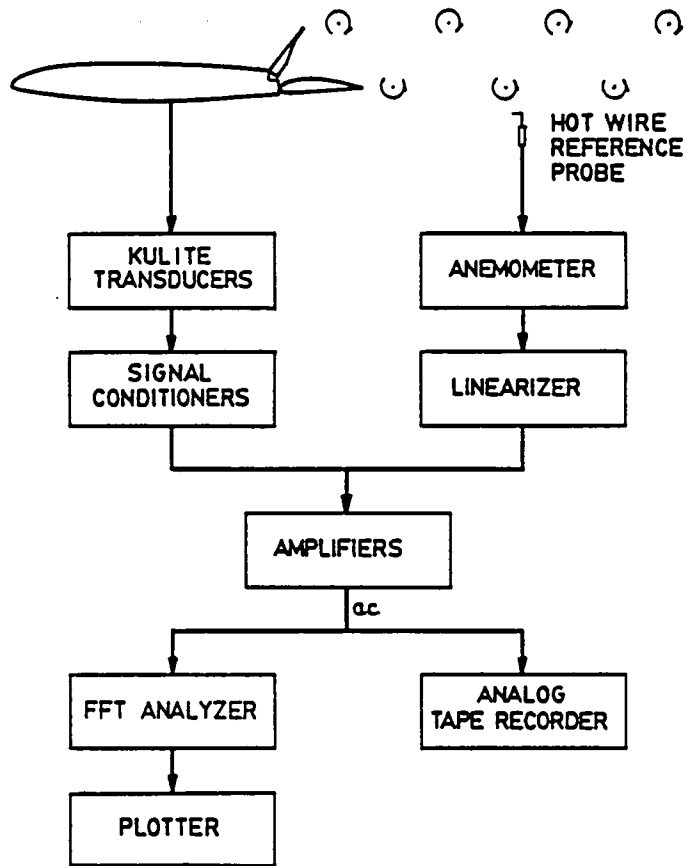
Figure D-3   Block diagram of fluctuating surface
             pressure measurement system.

Table D-3

Schlieren Flow Visualization
Heating Element Locations[*]

Chordwise Locations

Element No.	$\dfrac{X}{C}$
1	.700
2	.733
3	.793
4	.911

* Note: Nichrome wires buried spanwise in
the airfoil surface.

SCHLIEREN MIRROR

STROBE

TRIGGER

HOT-WIRE

WIND TUNNEL

VISUALIZATION
SCREEN

KNIFE
EDGE

SCHLIEREN MIRROR
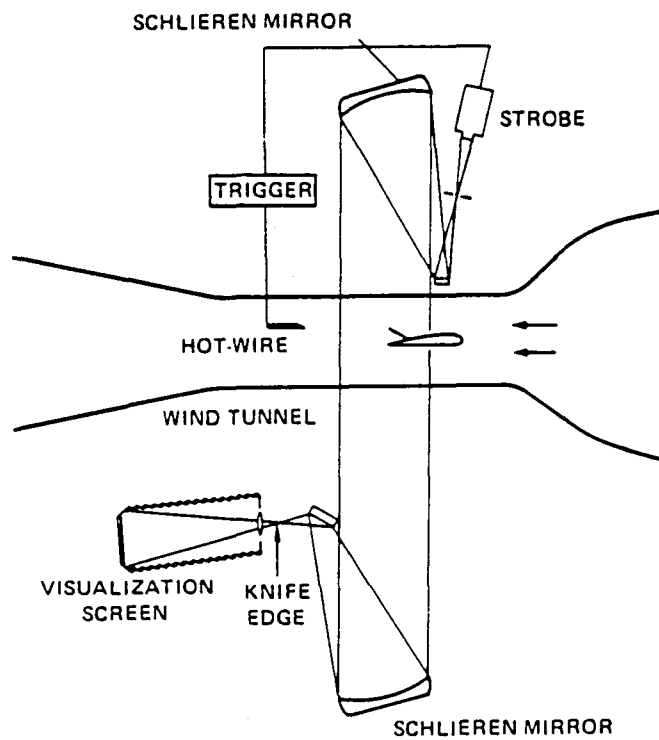
Figure D-4   Schematic of schlieren flow visualization
            system. Figure courtesy of S. Bodapati.

APPENDIX E

Data Reduction-Details

Presented in this section is a description of the data analysis. The items discussed and the order of presentation are as follows:

E-1 Analysis of Steady Flow Field Components

        E-1.1 Static Surface Pressure

        E-1.2 Boundary Layer Velocity Survey (hot-wire anemometry)

        E-1.3 Wake Velocity Survey (dual split film anemometry)

E-2 Analysis of Unsteady Flow Field Components

        E-2.1 Fluctuating Surface Pressure and Wake Velocity

        E-2.2 Determination of Vortex Shedding Frequency

E-1 Analysis of Steady Flow Field Components

The mean flow field data was processed into engineering units and coefficient form using a micro-computer (HP-9830A).

E-1.1 Static Surface Pressure

Data from the static surface pressure measurements was converted into coefficient form using the conventional scaling.

$$Cp = \frac{P\text{-}P_\infty}{q}$$

where
$$q = \text{free stream dynamic pressure}$$
$$P_\infty = \text{free stream static pressure (test section)}$$

The base pressure was calculated as the average of the static pressure measurements (5 total) made over the airfoil surface in the separated region aft of the spoiler: these measurements indicated the pressure to be nearly uniform.

48

The airfoil sectional lift and moment coefficients were found by numerically integrating the midspan chordwise static pressure distribution: no curve fitting was used, the trapezoidal rule was applied directly to the discrete data points of the static pressure distribution. The calculation is based on the following formulas:

<u>Lift Coefficient</u>

$$C_\ell = \left\{ \int_0^1 \Delta Cp \, d\tilde{x} \right\} \cos \alpha$$

<u>Moment Coefficient, about quarter chord</u>

$$Cm = \int_0^1 \Delta Cp(.25 - \tilde{x}) d\tilde{x}$$

where
$$\Delta Cp = Cp_{\text{lower surface}} - Cp_{\text{upper surface}}$$
$$\tilde{x} = \frac{x}{c}$$

The pitching-moment is calculated about the airfoil quarter chord point and is defined as nose-up positive.

The calculation of the increments of the lift and moment coefficients with spoiler deflection is based on the following formula:

$$\Delta Ci = \{Ci - Ci_{\delta=0}\}_{\alpha=\text{constant}}$$

where

$$i = \ell \text{ or } m$$

E-1.2 Boundary Layer Velocity Survey (hot-wire anemometry)

The boundary layer displacement thickness (δ^*), momentum thickness (θ), and shape factor (H) were calculated from the measured mean velocity profiles in conventional fashion:

$$\delta^* = \int_0^{Ze} \left(1 - \frac{U}{Ue}\right) dZ$$
$$\theta = \int_0^{Ze} \frac{U}{Ue}\left(1 - \frac{U}{Ue}\right) dZ$$
$$H = \delta^*/\theta.$$

Integration of the mean velocity profiles was performed using the trapezoidal rule: no curve fitting was performed, the trapezoidal rule was applied directly to the discrete data points of the mean velocity profile. An appropriate integration limit, the boundary layer thickness (Ze), was determined by visual inspection of the mean and r.m.s. velocity profiles.

The method of Kristensen was used to correct the mean velocity data for the variation in flow temperature between the measurement environment and that at calibration. Temperature correction factors, the ratio of the corrected to the uncorrected mean velocity, were estimated to range from 1 to .90, corresponding to temperature differences between the measurement and calibration environment of 0 C° to 10 C°, respectively.

No corrections were applied to account for hot-wire heat loss to the airfoil surface: visual inspection of the boundary layer velocity profiles, and calculations of corrections using the method of Wills, showed that corrections are negligible.

References

Kristensen, H.S., "Hot-wire Measurements in Turbulent Flows," DISA Information Department.

Wills, J.A.B., "The Correction of Hot-wire Readings for Proximity to a Solid Boundary," Journal of Fluid Mechanics, 12, pp 388-396, 1962.

E-1.3 Wake Velocity Survey (dual split film anemometry)

The mean velocity, mean flow angle, and two turbulence components were calculated; the data was corrected to take into account the difference in the flow temperature at calibration and that at measurement.

E-2 Analysis of Unsteady Flow Field Components

E-2.1 Fluctuating Surface Pressure and Wake Velocity

Spectral and correlation analysis was performed, using a fast Fourier transform analyzer (Nicolet 660B) and a direct computation correlator (Honeywell/Saicor SAI-

43A), respectively: reference may be made to Bendat et al. for a description of the digital computation procedures employed by both instruments. Power and RMS spectra were calculated, in engineering units, with a frequency resolution of 2.5 Hz over two frequency ranges (0 to 1 KHz and 2 KHz); auto/cross-correlations were calculated with a 400 point resolution over the time delay window selected. The calculations were ensemble averaged over the sampling time of the signal; based on the relationships to follow.

Spectral Analysis

Power Spectra $\quad G_{AA} = \overline{S_A S_A^*}$

RMS Spectra $\qquad = \sqrt{G_{AA}}$

where

$$S_A = \mathcal{F}\{A(t)\}$$
$$A(t) = \text{time signal}$$
$$\mathcal{F} = \text{Fast Fourier Transform (FFT)}$$
$$^* = \text{complex conjugate}$$

Correlation Analysis

$$R_{AB}(\tau) = \frac{1}{T} \int_0^T A(t)B(t+\tau)dt$$

where

$$T = \text{Sample (or Averaging) time interval}$$

E-2.2 Determination of Vortex Shedding Frequency

The determination of the existence of coherent[7] vortex shedding and its frequency was based on two criteria: One, displayed periodicity in the cross-correlation function between two points in the flow field (e.g. fluctuating pressure transducers on opposite sides of the airfoil); Two, the presence of a discrete "spike" in the spectra of the wake velocity field or surface pressure field. Furthermore, asymmetric vortex

---

[7]The term "coherent" is used here to denote the existence of a continuing relationship between any two points in the flow field.

shedding was confirmed by a 180° phase shift between the periodic (f) component of the pressure signals from two fluctuating pressure transducers (e.g., transducers 3 and 11, see Table D-2) located on opposite sides of the airfoil. Of note, is that the vortex shedding frequency is defined as that due to passage of one side of the vortex street.

References

Bendat, J.S., and Piersol, A.G., "Random Data: Analysis and Measurement Procedures," Chap. 9, John Wiley & Sons, 1971.

REFERENCES

The following list contains only those works to which reference is made in the text. Of note, is that those works referenced in the appendices are listed at the end of the section where referenced.

1. Hoerner, S. F., and Borst, H. V., "Fluid Dynamic Lift," Published by Hoerner Fluid Dynamics, 1975, pg. 10-14.

2. Jones, B., "Elements of Practical Aerodynamics" John Wiley & Sons, Inc., New York, 1939, pg. 414.

3. — , "Aerodynamic Characteristics of Controls," AGARD C.P. No. 262, 1979.

4. Ostgaard, M. A., and Swortzel, F. R., "CCVs Active Control Technology Creating New Military Aircraft Design Potential," Astronautics & Aeronautics, February 1977.

5. Dryden Flight Research Center, "Advanced Control Technology and its Potential for Future Transport Aircraft," NASA TM X-3409, August 1976.

6. — , "Impact of Active Control Technology on Airplane Design," AGARD C.P.-157, October 1974.

7. Siddalingappa, S. R., and Hancock, G. J., "An Introduction to the Aerodynamics of Spoilers," Dept of Aero. Eng., Queen Mary College, Univ. of London, QMC EP-1034, August 1980.

8. Mack, M. D., Seetharam, H. C., Kuhn, W. G., and Bright, J. T., "Aerodynamics of Spoiler Control Devices," AIAA Paper 79-1873, AIAA Aircraft Systems and Technology Meeting, New York, N.Y., August 1979.

9. Weick, F. E., and Jones, R. T., "Resume and Analysis of N.A.C.A. Lateral Control Research," NACA Report No. 605, 1937.

10. Weick, F. E., and Shortal, J. A., "Wind-Tunnel Research Comparing Lateral Control Devices Particularly at High Angles of Attack V – Spoilers and Ailerons on Rectangular Wings," NACA Report No. 439, 1932.

11. Wentz, W. H., Ostowari, C., and Seetharam, H. C., "Effects of Design Variables on Spoiler Control Effectiveness, Hinge Moments and Wake Turbulence, " AIAA Paper 81-0072, AIAA 19th Aerospace Sciences Meeting, St. Louis, Missouri, Jan. 1981.

12. Ayoub, A., Satyanarayana, B., Karamcheti, K., and Seetharam, H. C., "Unsteady Flow Patterns Associated with Spoiler Control Devices," AIAA Paper 82-0127, AIAA 20th Aerospace Sciences Meeting, Orlando, Florida, Jan. 1982.

13. McLachlan, B. G., Karamcheti, K., and van Leynseele, F., "Experimental Study of the Flowfield of an Airfoil with Deflected Spoiler", AIAA Paper 82-0126, AIAA 20th Aerospace Sciences Meeting, Orlando, Florida, Jan. 1982.

14. Smith, C. A., "Features of a Wake Tone Flow Field," Ph.D. Dissertation, Department of Aeronautics and Astronautics, Stanford University, June 1978.

15. Digumarthi, R. V., Koutsoyannis, S. P., and Karamcheti, K., "Some Observations of Surface Pressures and the Near Wake of a Blunt Trailing Edge Airfoil," Joint Institute for Aeronautics and Acoustics TR-39, Department of Aeronautics and Astronautics, Stanford University, June 1981.

16. von Doenhoff, A. E., and Tetervin, N., "Determination of General Relations for the Behavior of Turbulent Boundary Layers," NACA Report No. 772, 1943.

17. Allen, H. J., and Vincenti, W. G.,"Wall Interference in a Two-Dimensional-Flow Wind Tunnel, with consideration of the Effect of Compressibility," NACA Report No. 782, 1944.

18. Morkovin, M.V., "Flow Around Circular Cylinder - A Kaleidoscope of Challenging Fluid Phenomena," ASME-Symp. on Fully Separated Flows, Philadelphia, PA., May 1964.

19. Berger, E., and Wille, R., "Periodic Flow Phenomena," Annual Review of Fluid Mechanics, Vol. 4, 1972, pg 313-340.

20. Roshko, A., "On the Drag and Shedding Frequency of Two-Dimensional Bluff Bodies," NACA Tech. Note 3169, July 1954.

21. Roshko, A., "On the Wake and Drag of Bluff Bodies," J. of the Aeronautical Sciences, Vol. 22, February 1955.

22. Fage, A., and Johansen, F. C., "The Structure of Vortex Sheets, "Philosophical Magazine, S.7, Vol. 5, No. 28, February 1928.

23. Fage, A., and Johansen, F. C., "On the Flow of Air behind an Inclined Flat Plate of Infinite Span," Proc. Roy. Soc. (London), Ser. A., Vol. 116, No. 773, September 1, 1927.

24. Wenzinger, C. J., "Wind-Tunnel Investigation of Ordinary and Split Flaps on Airfoils of Different Profile," NACA Report No. 554, 1936.

25. Wenzinger, C. J., and Harris, T. A., "Pressure Distribution over a Rectangular Airfoil with a Partial-Span Split Flap," NACA Report No. 571, 1936.

26. Wallace, R., "Investigation of Full-Scale Split Trailing-Edge Flaps with Various Chords and Hinge Locations," NACA Report No. 539, 1935.

27. Bursnall, W. J., and Loftin, L. K., "Experimental Investigation of Localized Regions of Laminar-Boundary-Layer Separation," NACA Tech. Note 2338, April 1951.

28. Gault, D. E., "An Experimental Investigation of Regions of Separated Laminar Flow," NACA Tech. Note 3505, September 1955.

29. Chapman, D. R., Kuehn, D. M., and Larson, H. K., "Investigation of Separated Flows in Supersonic and Subsonic Streams with Emphasis on the Effect of Transition," NACA Tech. Note 3869, March 1957.

30. Dryden, H. L., "Some Recent Contributions to the Study of Transition and Turbulent Boundary Layers," NACA Tech. Note 1168, April 1947.

BIBLIOGRAPHY

Aerodynamics of Spoilers

Extensive reference lists on the aerodynamics of spoilers are contained in the following works.

Hoerner, S. F., and Borst, H. V., "Fluid-Dynamic Lift," Published by Hoerner Fluid Dynamics, 1975, pg 10-14 - 10-22.

Hoerner, S. F., "Fluid-Dynamic Drag," Published by Hoerner Fluid Dynamics, 1965, pg 13-11 - 13-13.

Mack, M. D., Seetharam, H. C., Kuhn, W. G., and Bright, J. T., "Aerodynamics of Spoiler Control Devices," AIAA Paper 79-1873, AIAA Aircraft Systems and Technology Meeting, New York, N.Y., August 1979.

Roskam, J., Kohlman, D.L., and Wentz, W. H., "Spoilers for Roll Control of Light Airplanes," AIAA Paper 74-861, AIAA Mechanics and Control of Flight Conference, Anaheim, California, August 1974.

Siddalingappa, S. R., and Hancock, G. J., "An Introduction to the Aerodynamics of Spoilers," Dept. of Aero. Eng., Queen Mary College, Univ. of London, QMC EP-1034, August 1980.
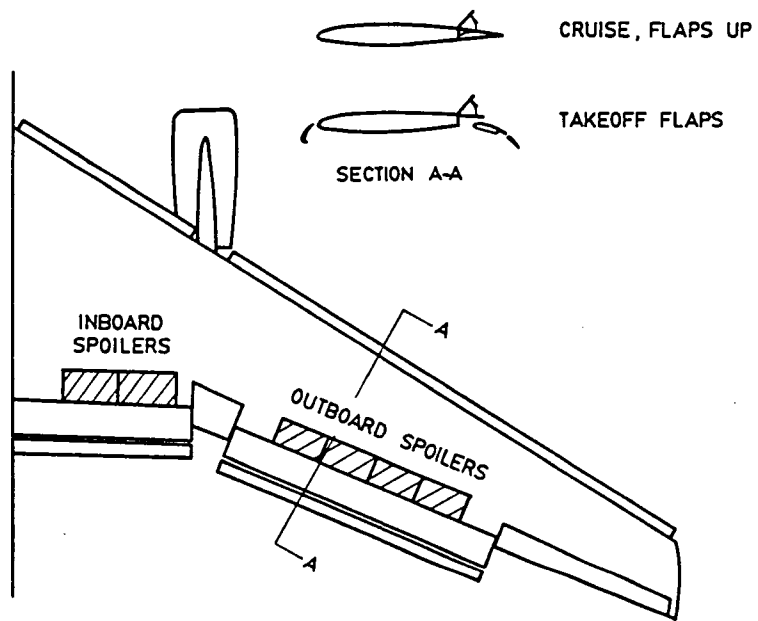
Figure 1.1 Plan view of typical transport spoiler
            configuration.
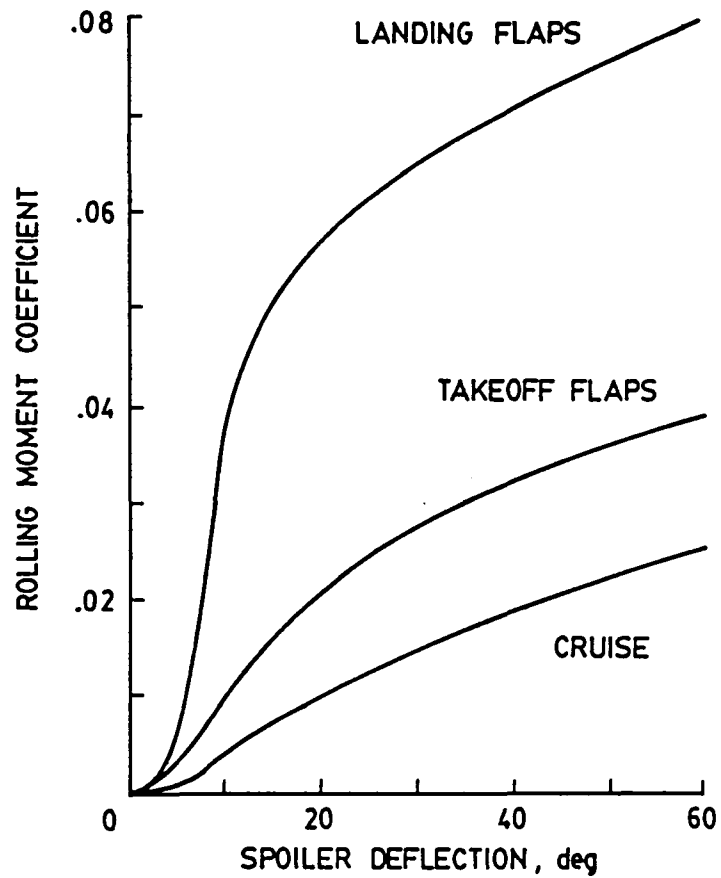
Figure 1.2 Typical transport spoiler control effectiveness
characteristics. Shown are three flap deflection
settings: cruise < takeoff < landing. Data is for
a DC-9-30, courtesy of R.S. Shevell.

CONSTANT SPEED (19 Hz)
VARIABLE PITCH FAN (16 BLADES)
FAN MOTOR (20 hp)
NACELLE

TURNING VANES

BREATHER VENT

TEST SECTION
AIRSPEED RANGE 19-65 m/s
TURBULENCE LEVEL < 1%

TURBULENCE
DAMPING SCREENS
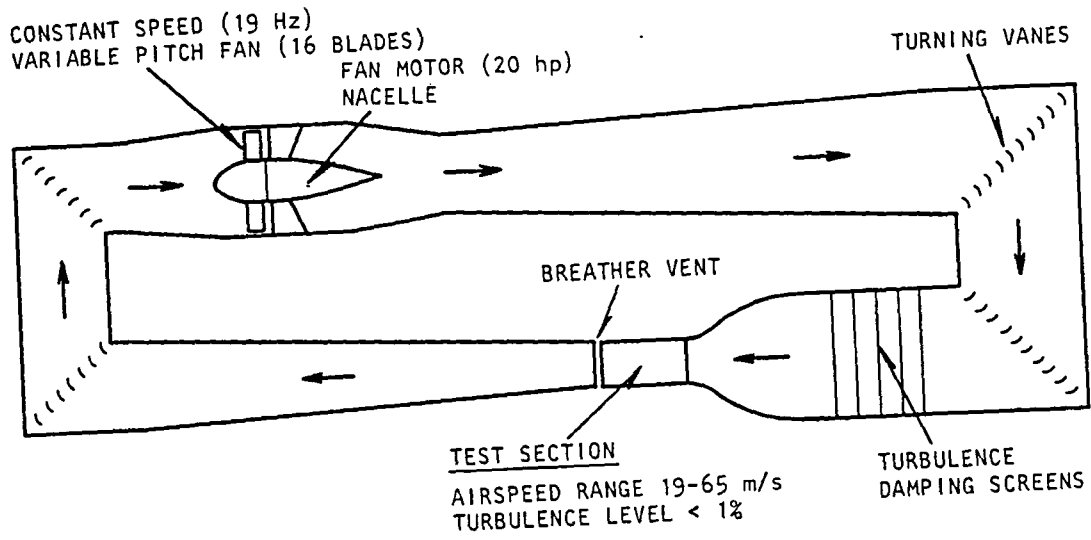
Figure 2.1 Wind tunnel plan view.

60

AIRFOIL PARAMETERS
CHORD — 8 in. (0.2032 m)
THICKNESS — 0.113 c
SPOILER CHORD — 0.1554 c
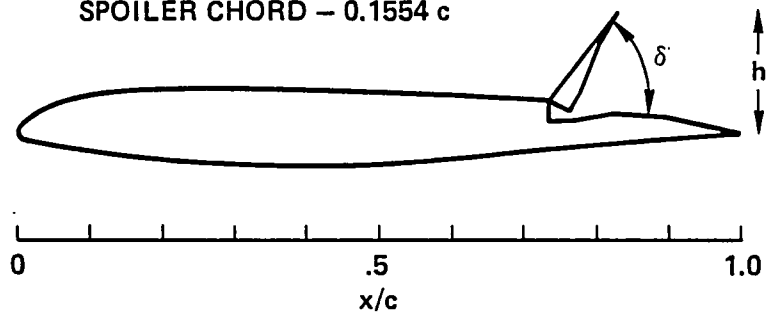
Figure 2.2 Airfoil geometry and parameters.

61
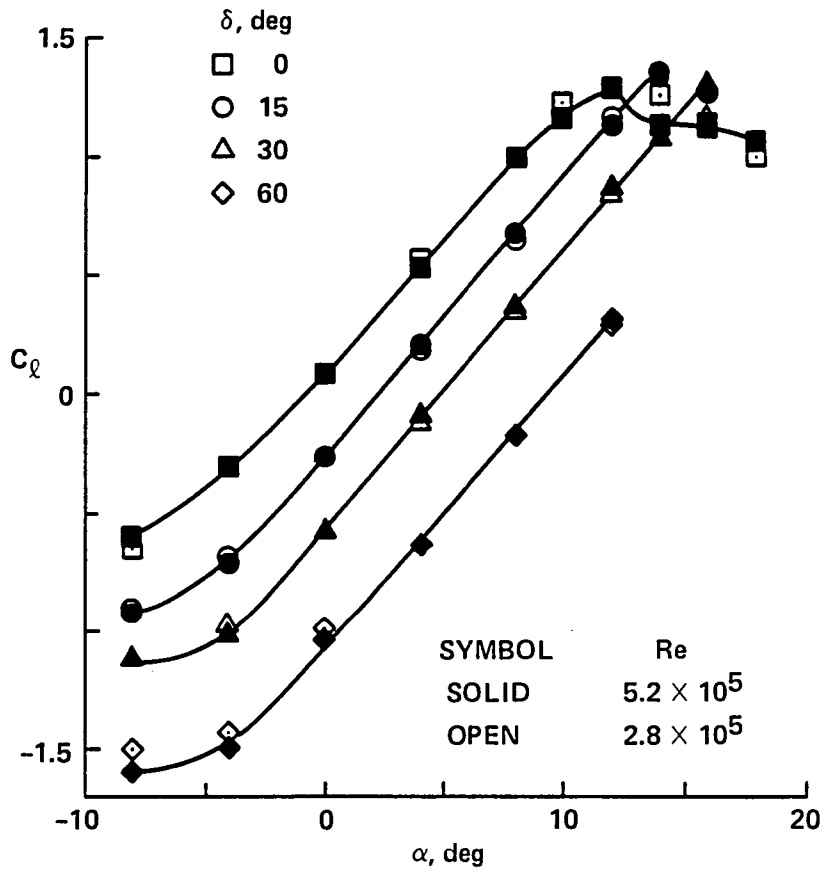
Figure 3.1 Airfoil lift characteristics.
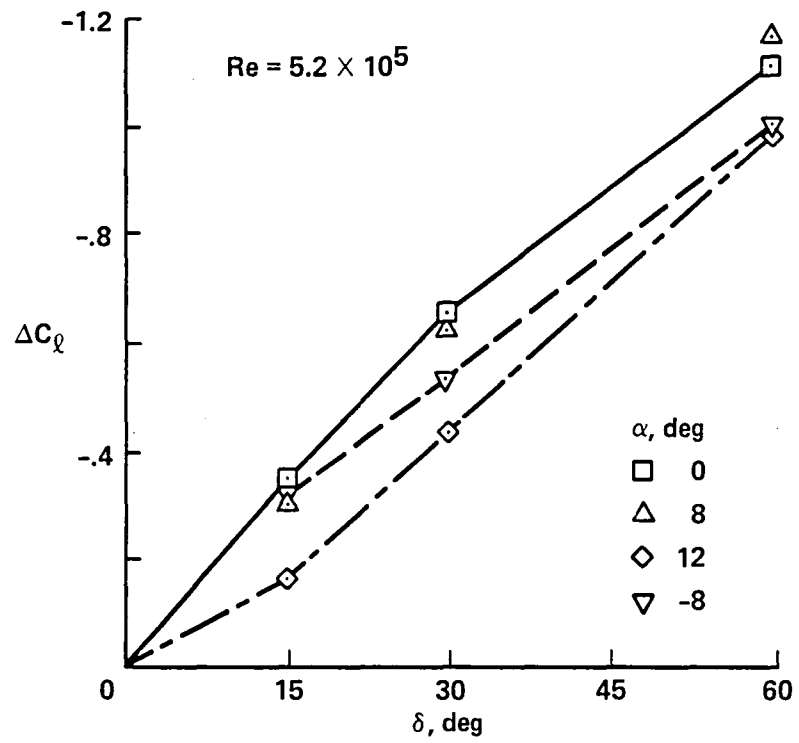
Figure 3.2 Lift increment as a function of spoiler
deflection.

63
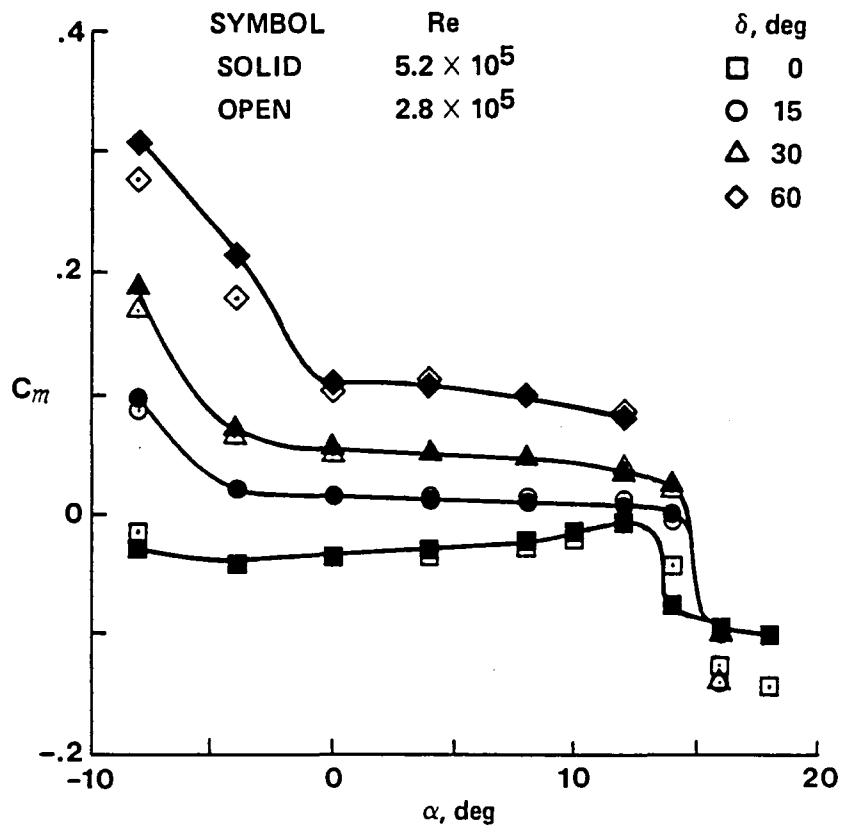
Figure 3.3 Airfoil pitching-moment characteristics.
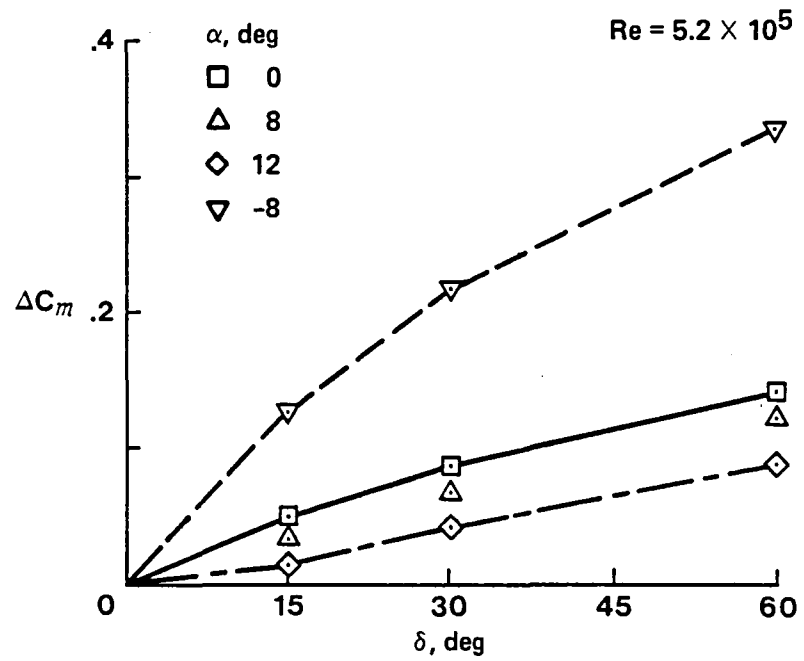
Figure 3.4 Pitching-moment increment as a function of
spoiler deflection.
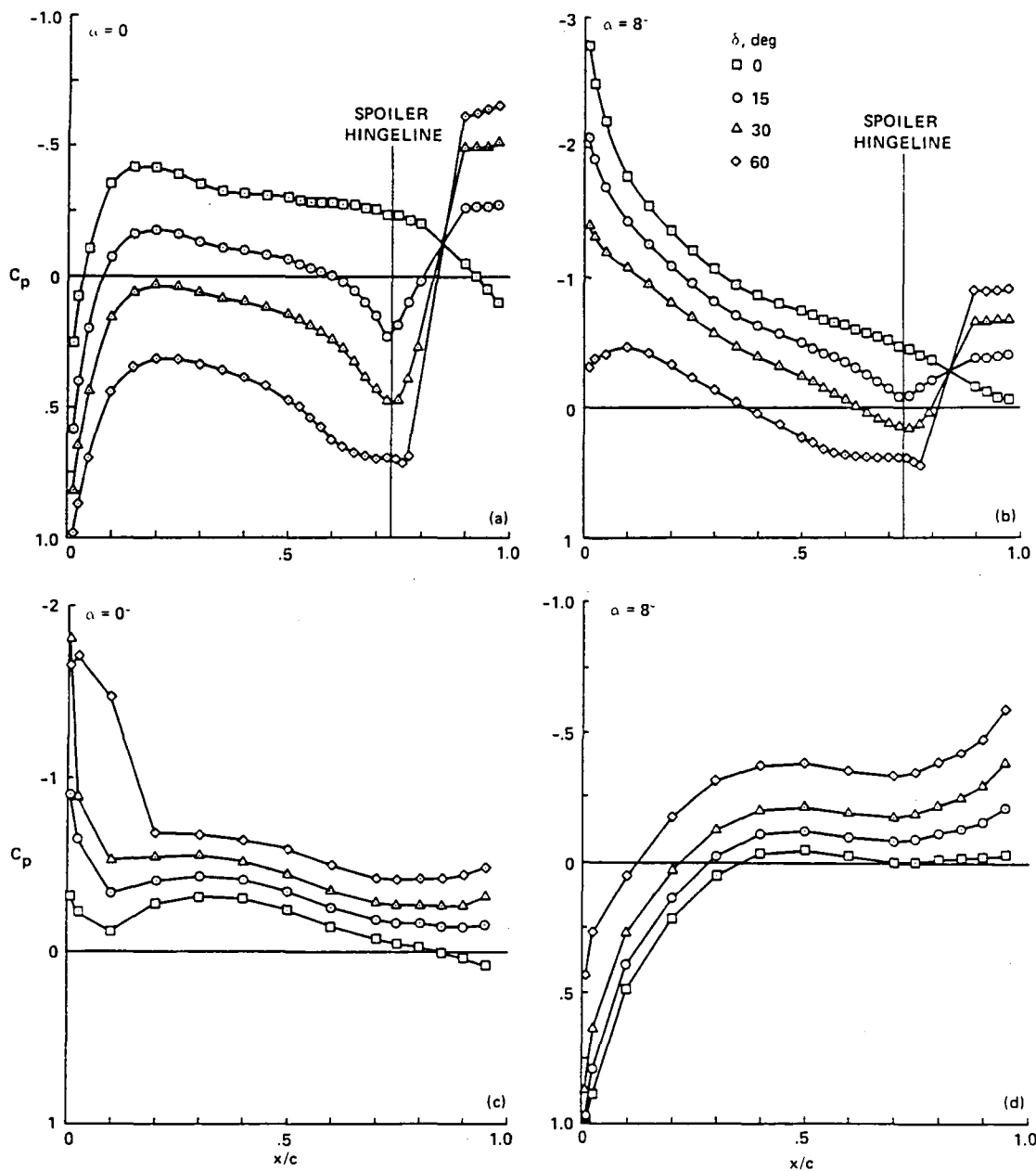
Figure 3.5   Effect of spoiler deflection on surface pressure
distribution: upper surface (a) and (b), lower
surface (c) and (d); Re = 5.2 x 10^5.
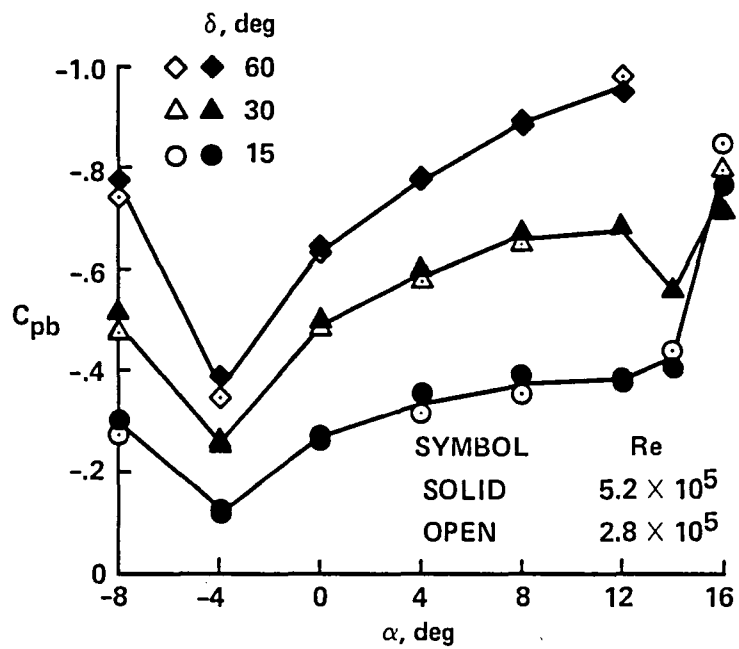
Figure 3.6 Base pressure coefficient.
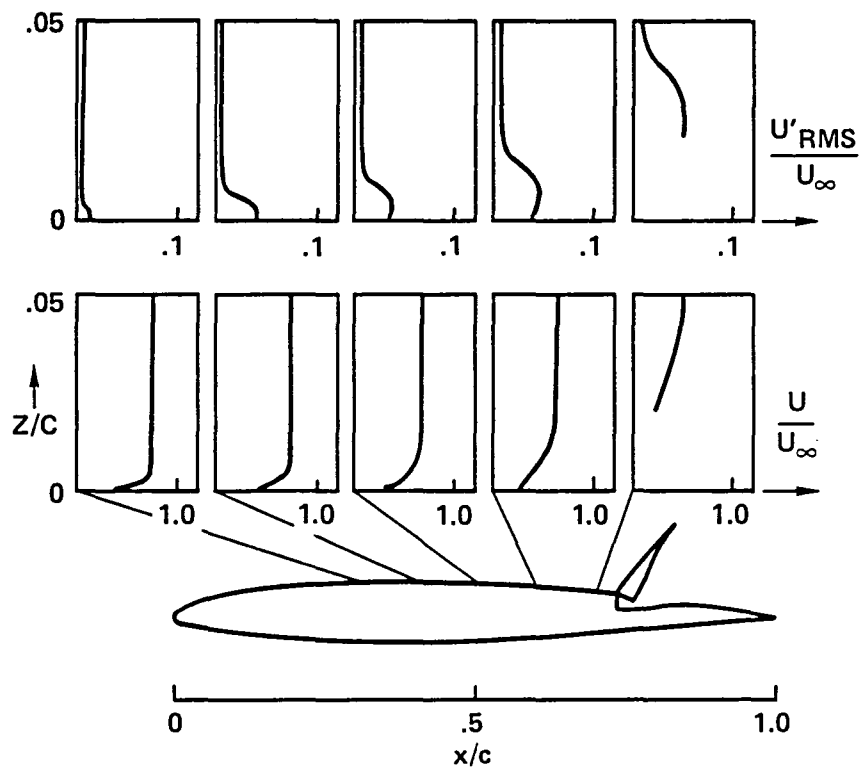
Figure 3.7   Boundary layer velocity profiles (mean and
             r.m.s.): Re = 5.2 x 10^5, α = 0°, δ = 60°.
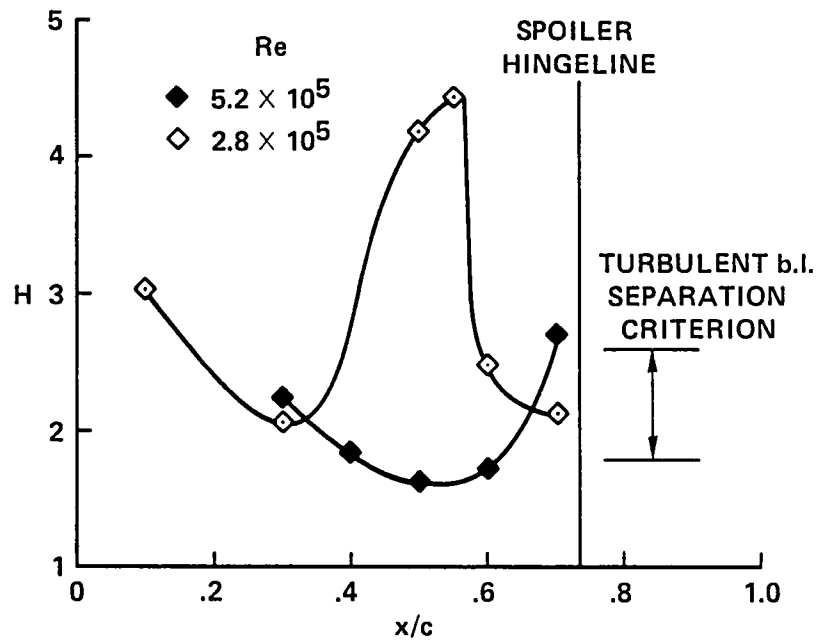
Figure 3.8   Effect of Reynolds number on the boundary
layer shape factor (upper surface):
$\delta = 60°$, $\alpha = 0°$. Turbulent boundary
layer (Re = 5.2 x 10^5), transitional
boundary layer (Re = 2.8 x 10^5).
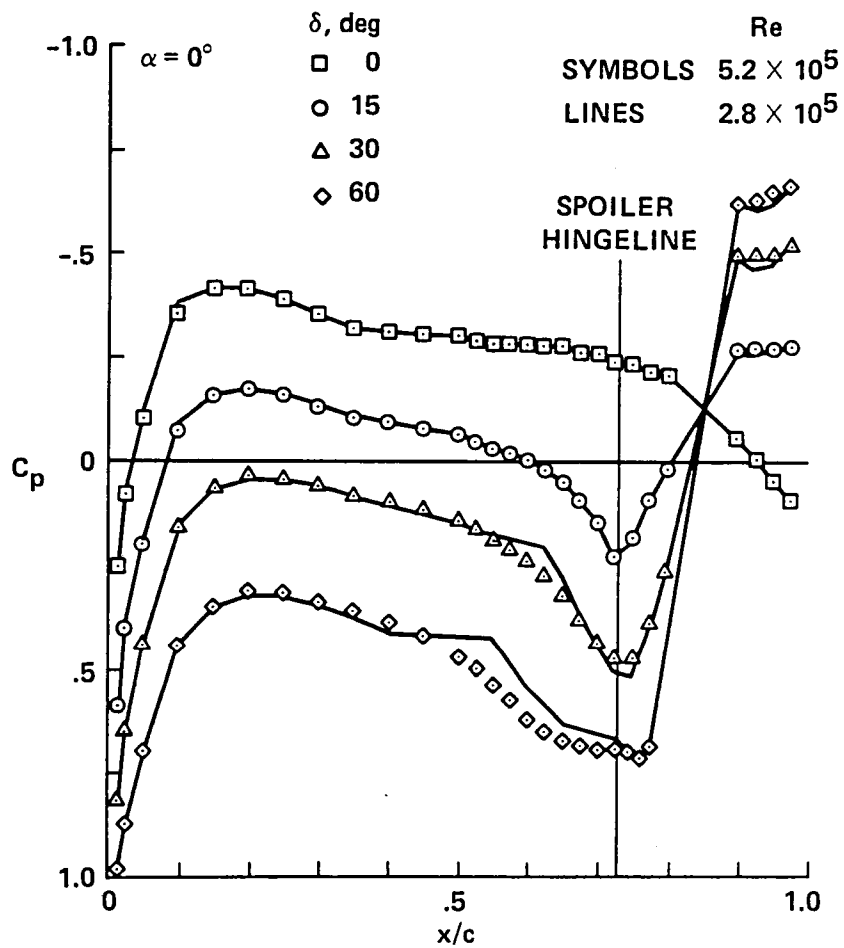
Figure 3.9 Effect of Reynolds number on the upper surface
pressure distribution.
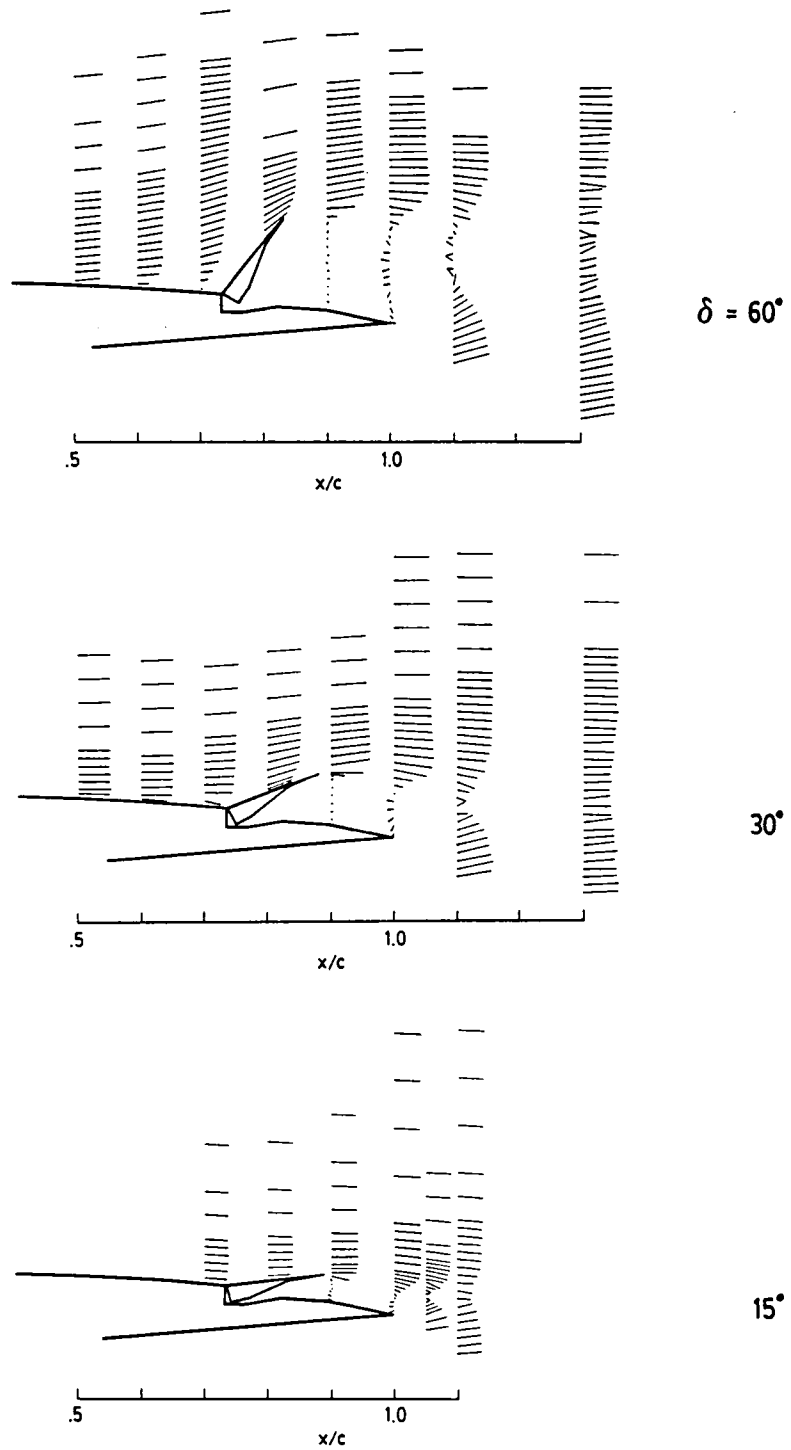
Figure 3.10 Mean velocity vector plots of the near
            wake: Re = 2.8×10^5, $\alpha = 0°$.

72
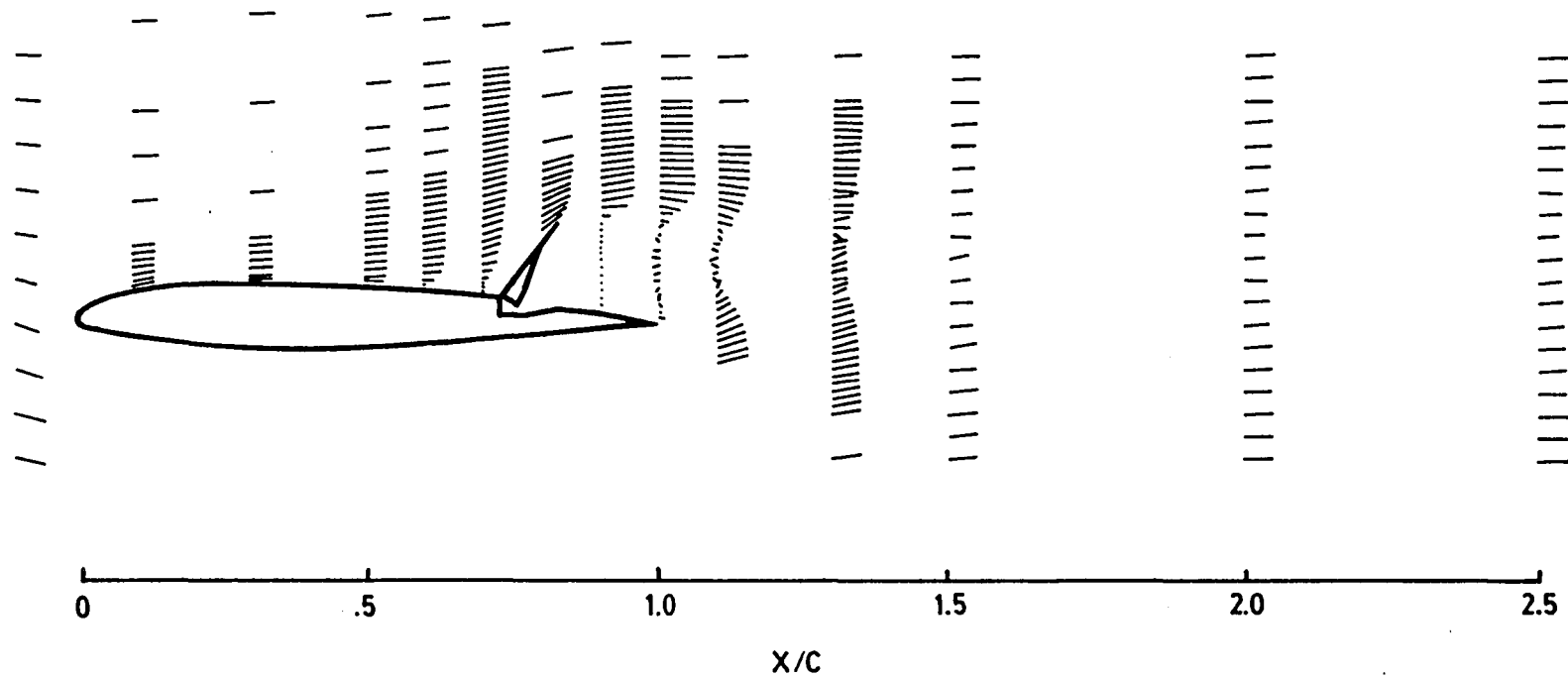
Figure 3.11a   Mean velocity vector plots of the overall flow
field: Re = 2.8×10^5, $\delta = 60°$, $\alpha = 0°$.

X/C

73
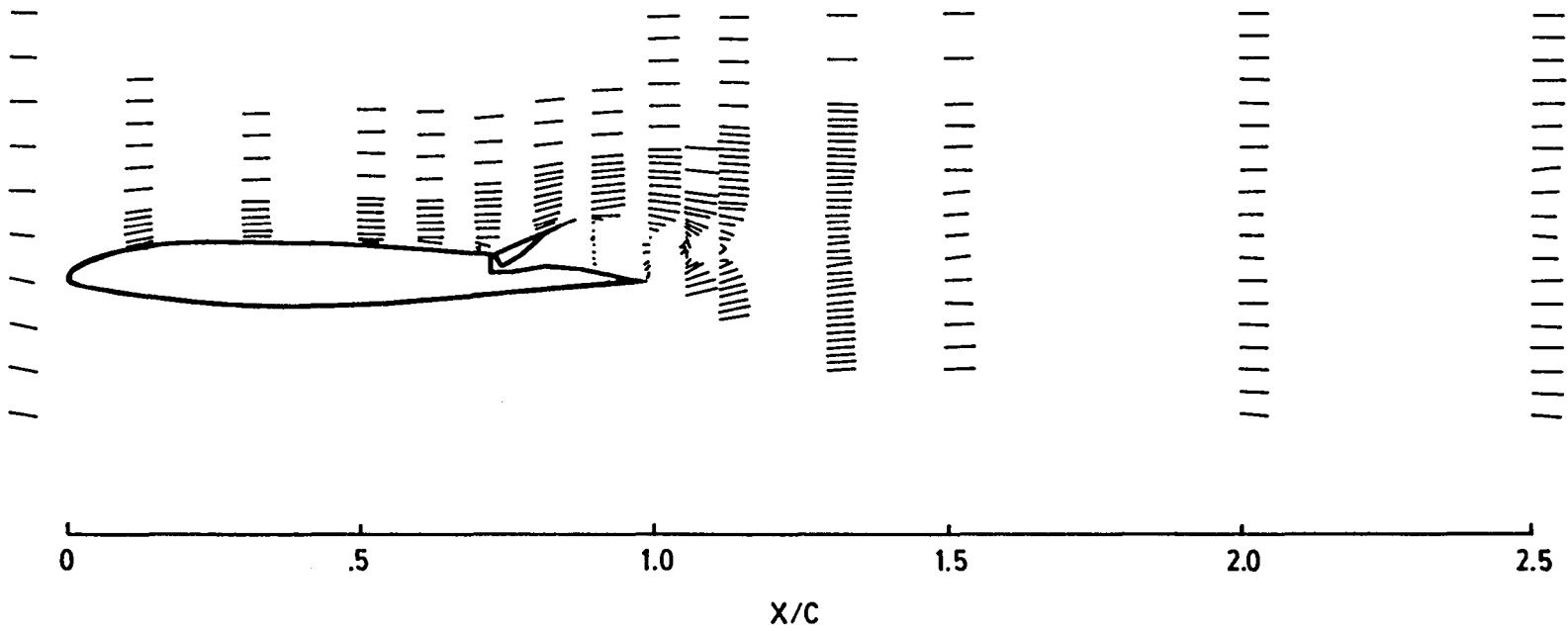
Figure 3.11b Mean velocity vector plots of the overall flow
field: Re = 2.8 x 10^5, δ = 30°, α = 0°.

X/C

X/C
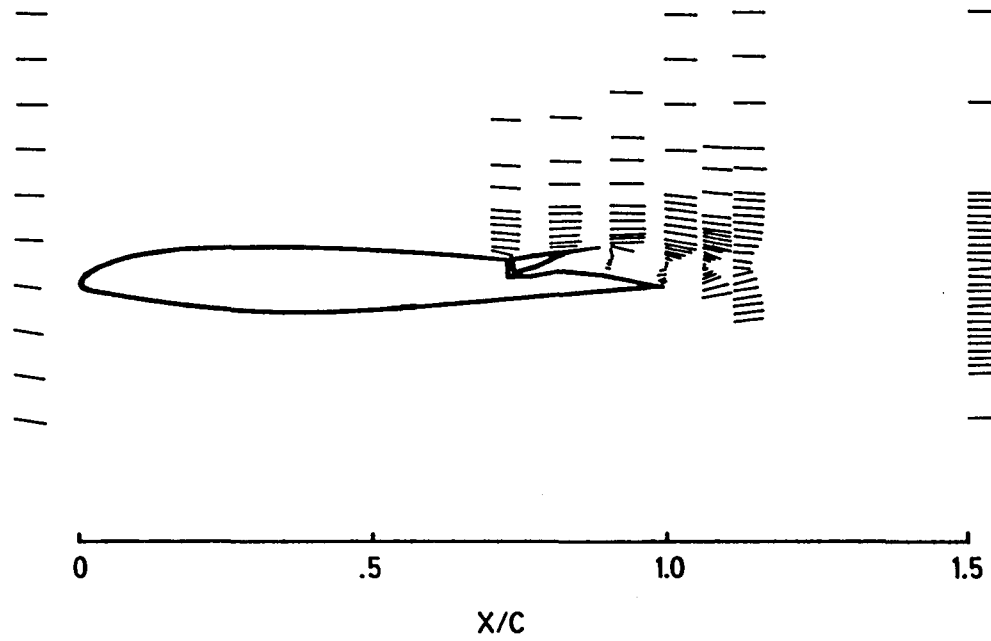
Figure 3.11c Mean velocity vector plots of the overall flow
field: Re = 2.8 x 10^5, δ = 15°, α = 0°.
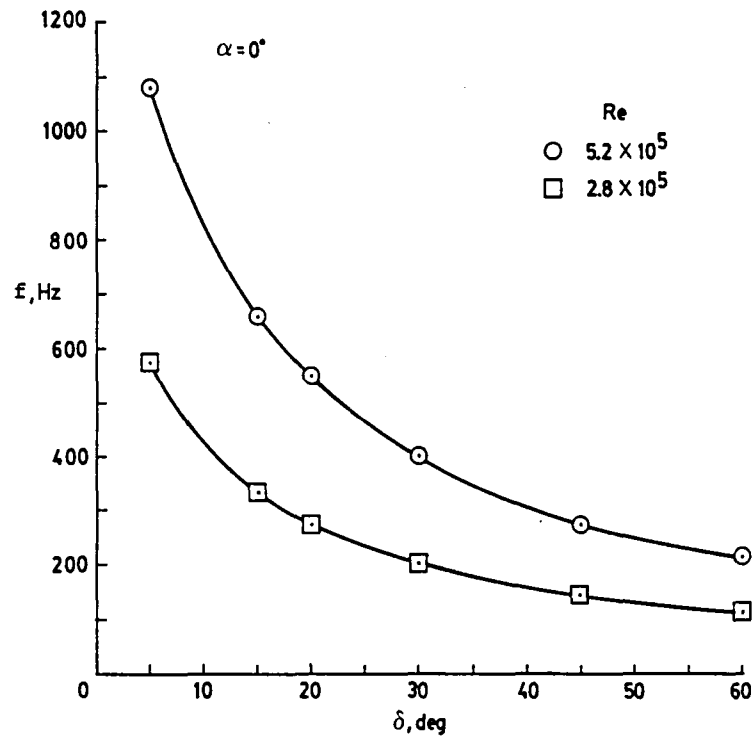
Figure 3.12 Vortex shedding frequency as a function of spoiler deflection.
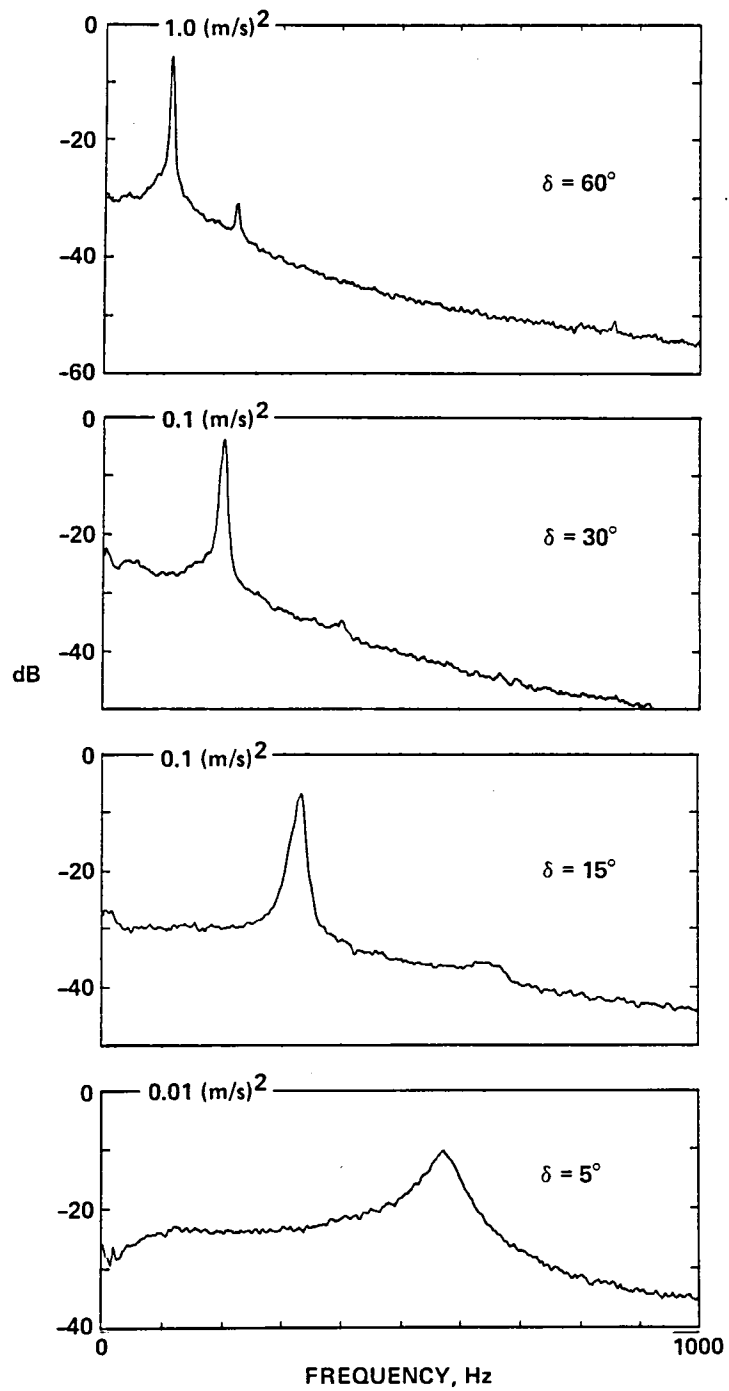
Figure 3.13   Effect of spoiler deflection on wake
power spectra: Re = 2.8 x 10^5, α = 0°.
Obtained using hot-wire at lower edge
of wake, x/c = 1.6.

76
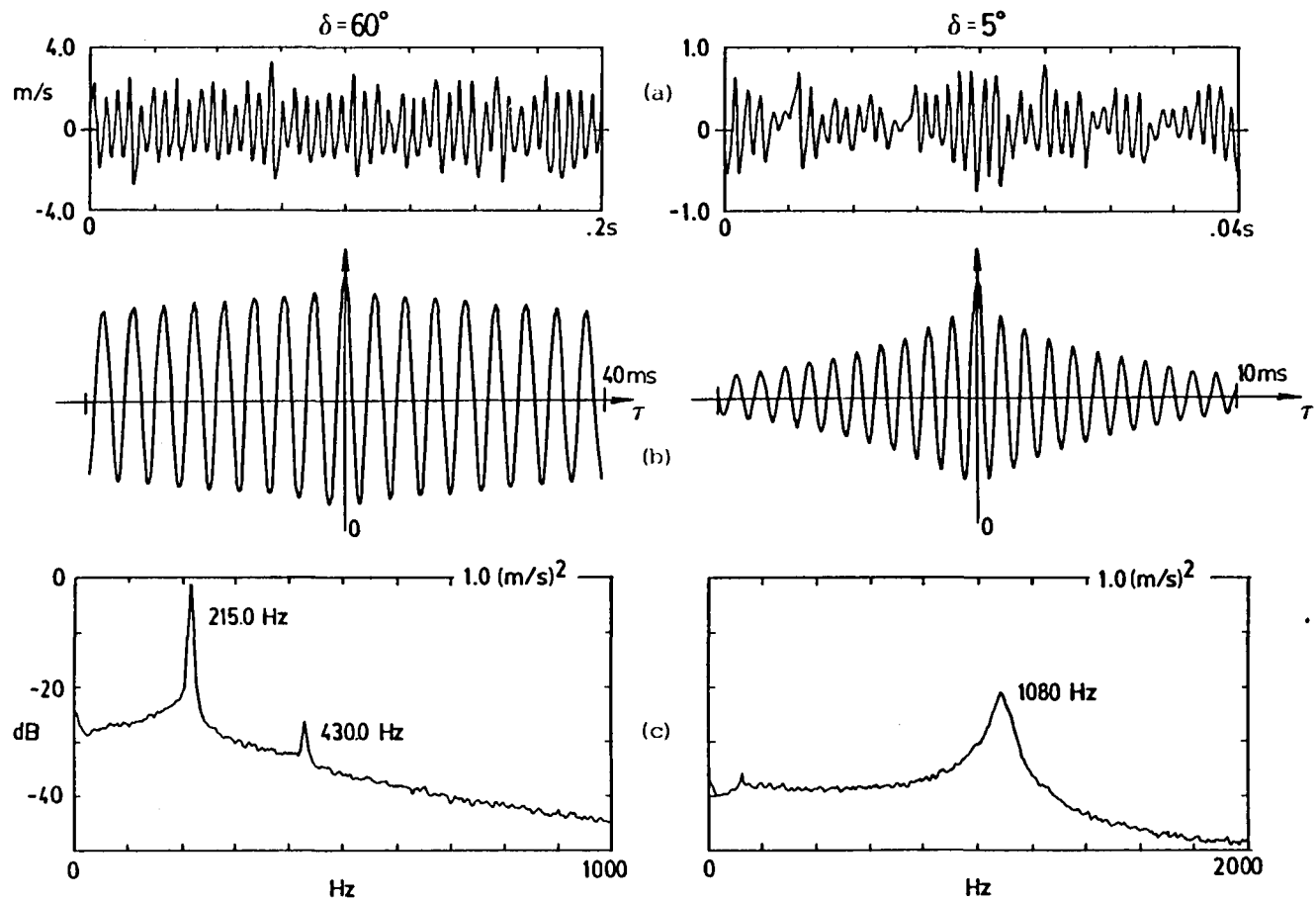
Figure 3.14 (a) Signal, (b) Auto-correlation, (c) Power spectra of wake velocity fluctuations: Re = 5.2 x 10^5, α = 0°. Obtained using hot-wire at lower edge of wake, x/c = 1.6.
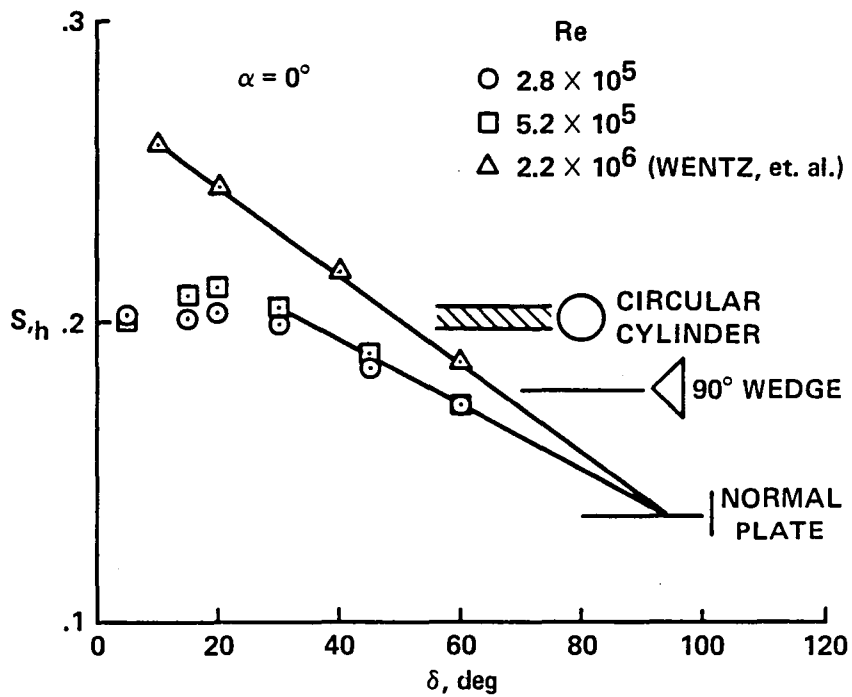
Figure 3.15   Strouhal number (based on the spoiler projection
height) as a function of spoiler deflection. Bluff
body Strouhal number values are from reference 20.
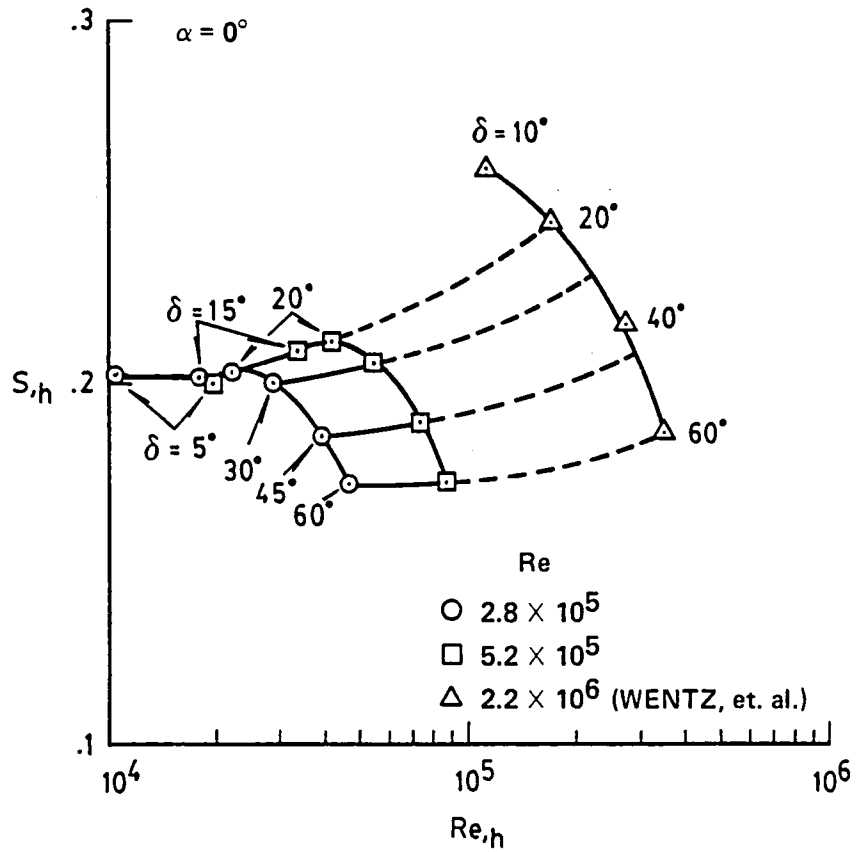
Figure 3.16 Strouhal number as a function of Reynolds number (both based on the spoiler projection height).

79
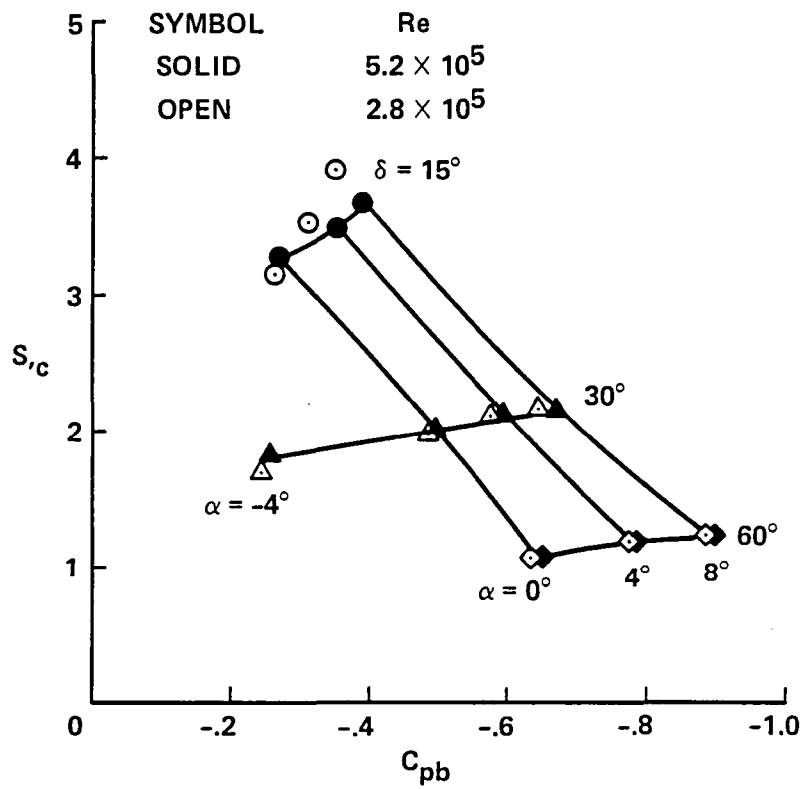
Figure 3.17 Strouhal number (based on airfoil chord) as
a function of base pressure coefficient.
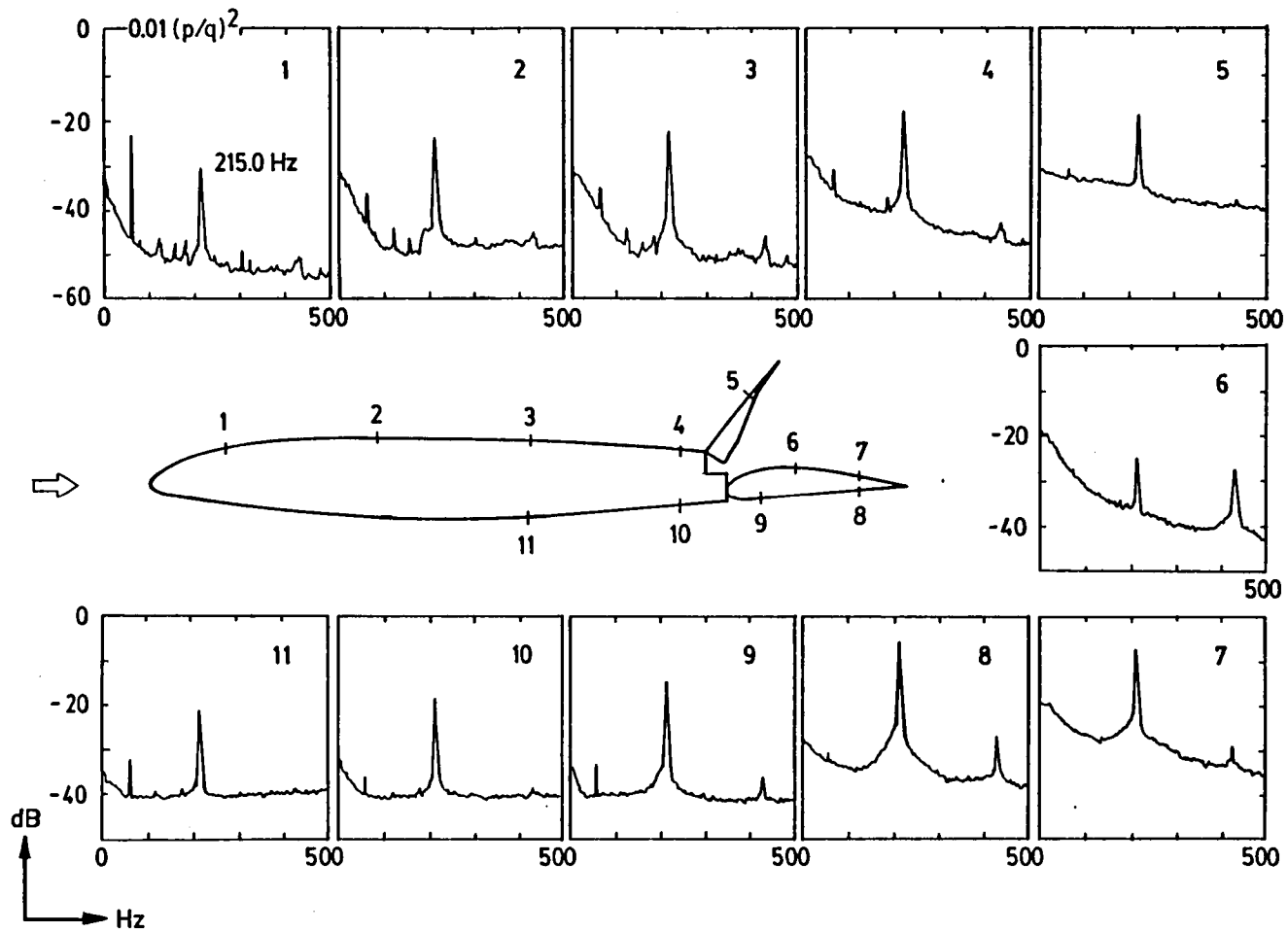
Figure 3.18   Surface pressure power spectra:
Re = 5.2 x 10⁵, δ = 60°, α = 0°.
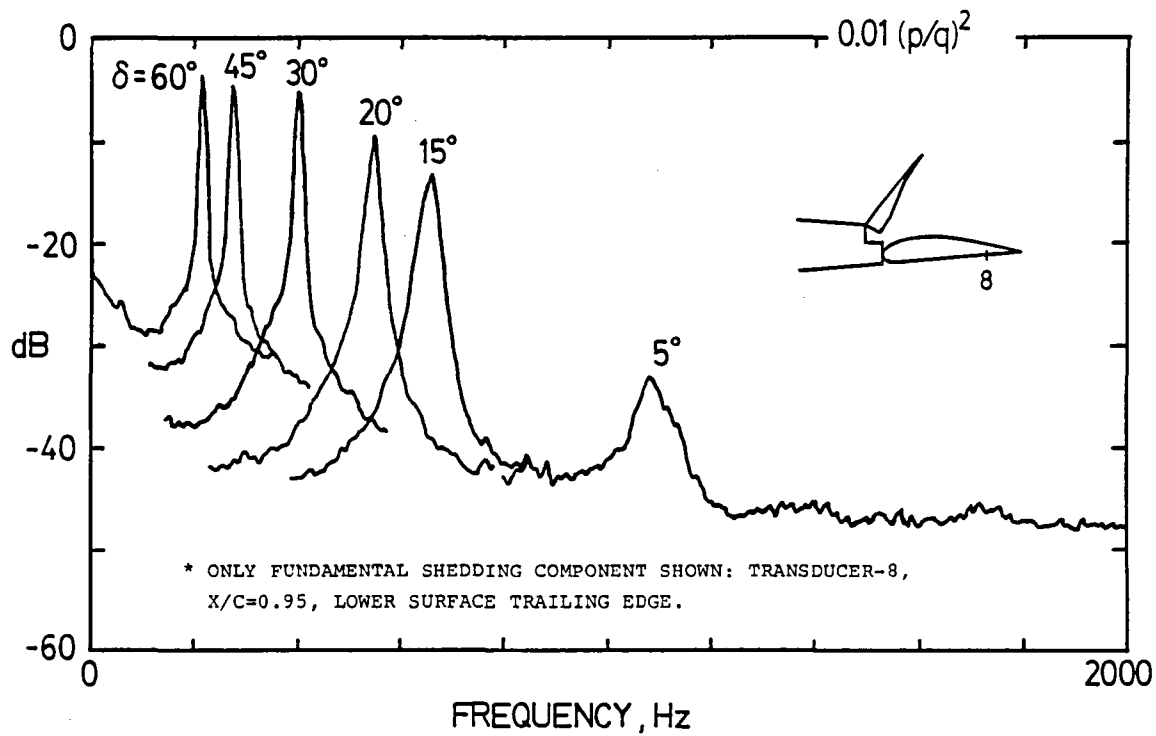
Figure 3.19 Effect of spoiler deflection on surface pressure power
spectra: Re = 5.2 x 10^5, α = 0°.
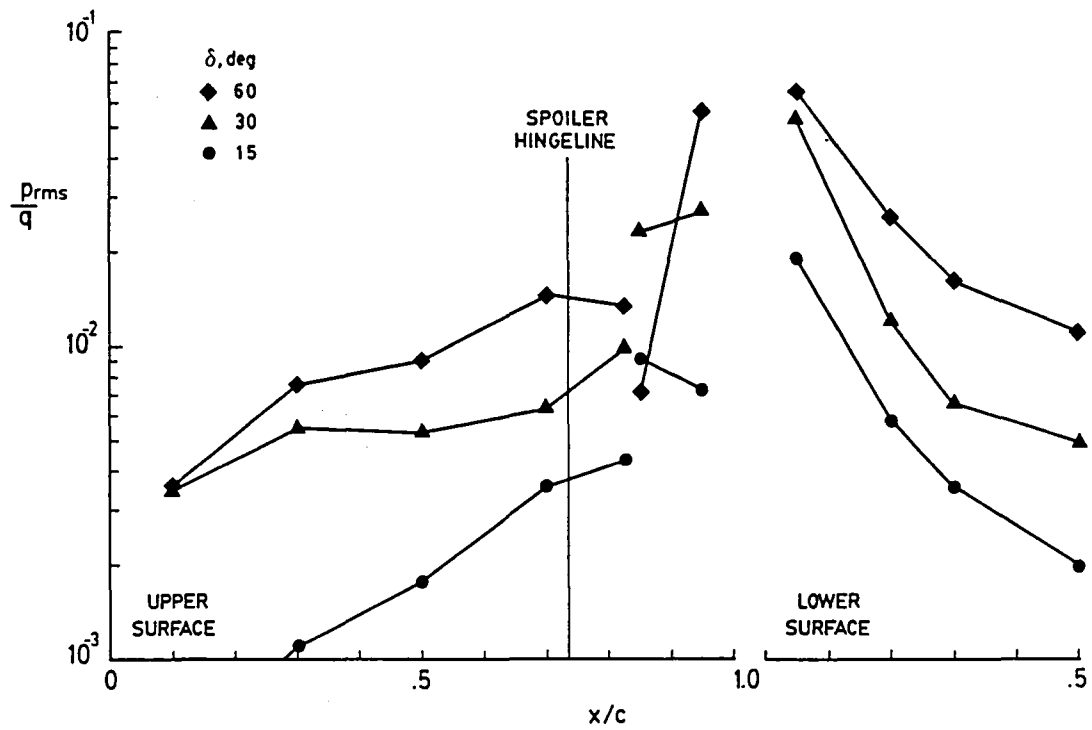
Figure 3.20   Effect of spoiler deflection on fluctuating pressure
              coefficient distribution (f component): Re = 5.2 x 10^5,
              α = 0°.
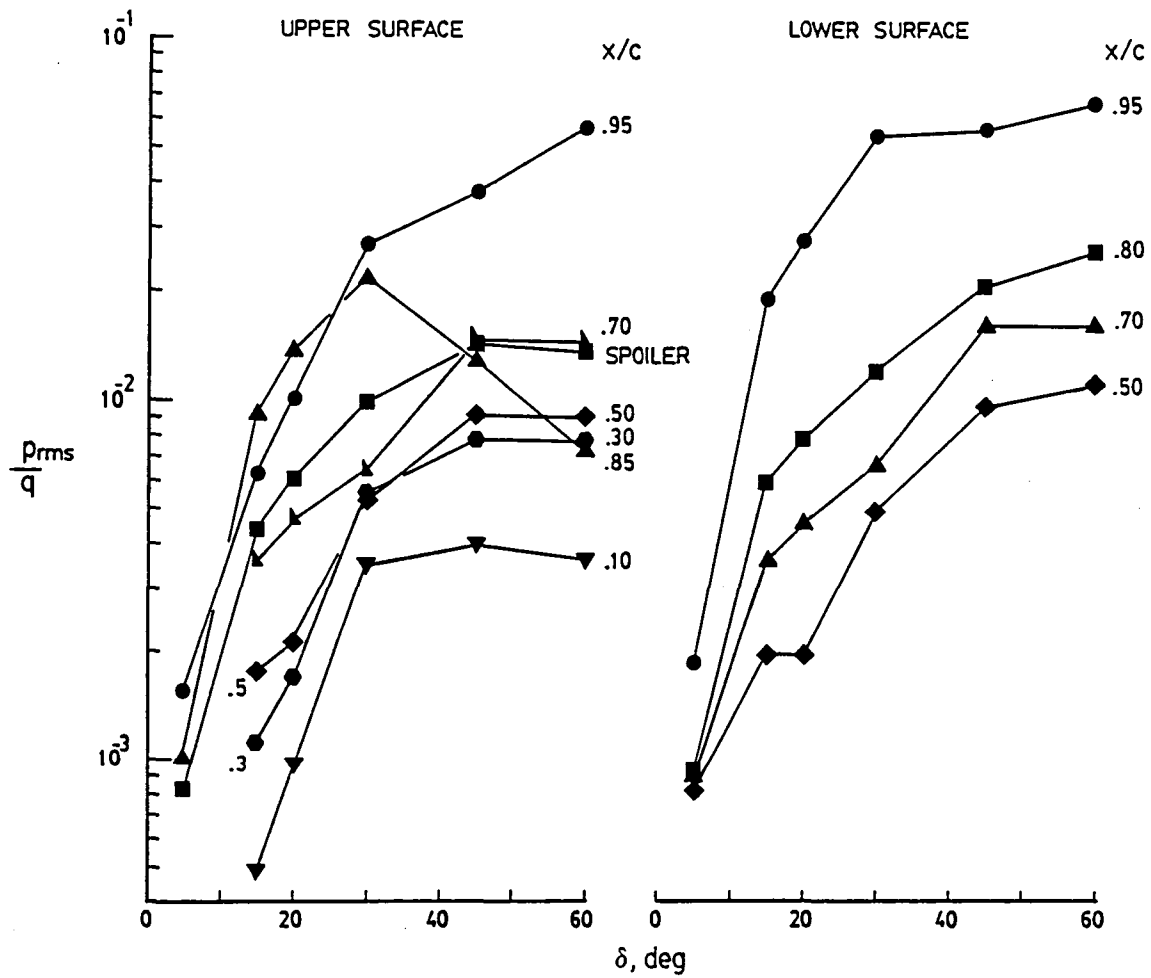
Figure 3.21   Fluctuating pressure coefficient (f component) as
              a function of spoiler deflection: Re = 5.2 x 10^5,
              α = 0°.
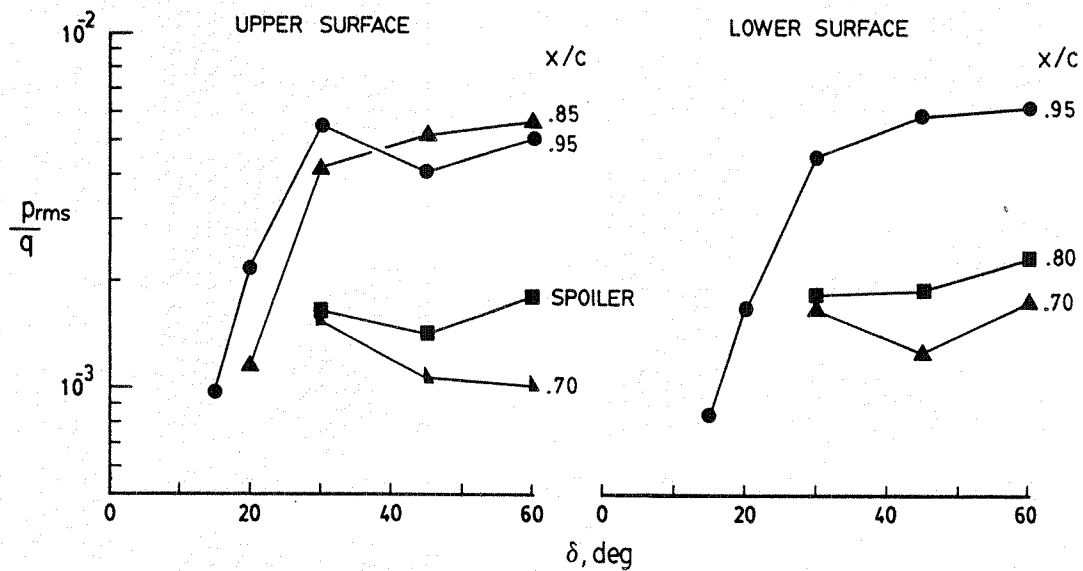
Figure 3.22 Fluctuating pressure coefficient (2f component) as
a function of spoiler deflection: Re = 5.2 x 10^5,
α = 0°.

$\phi = 0°$ 36° 45° 72°

108° 144° 180° 216°

252° 288° 324° 360°
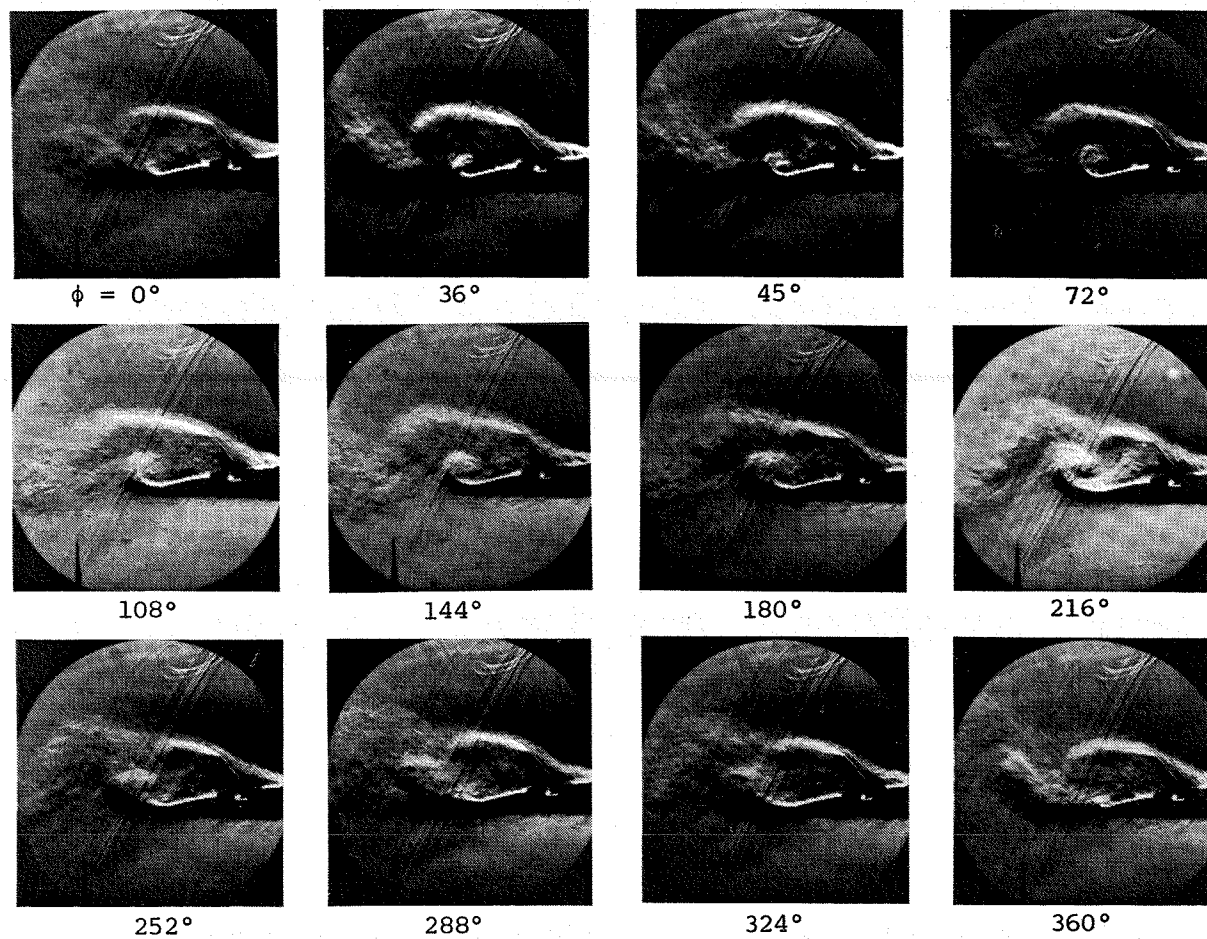
Figure 3.23a Phase locked schlieren flow visualization of the near wake (flow is from right to left): $\delta = 60°$, $\alpha = 0°$, Re = 2.3 x 10^5.

Figure 3.23b   Phase locked schlieren flow visualization of the near wake (flow is from right to left): $\delta = 30°$, $\alpha = 0°$, $Re = 2.3 \times 10^5$.
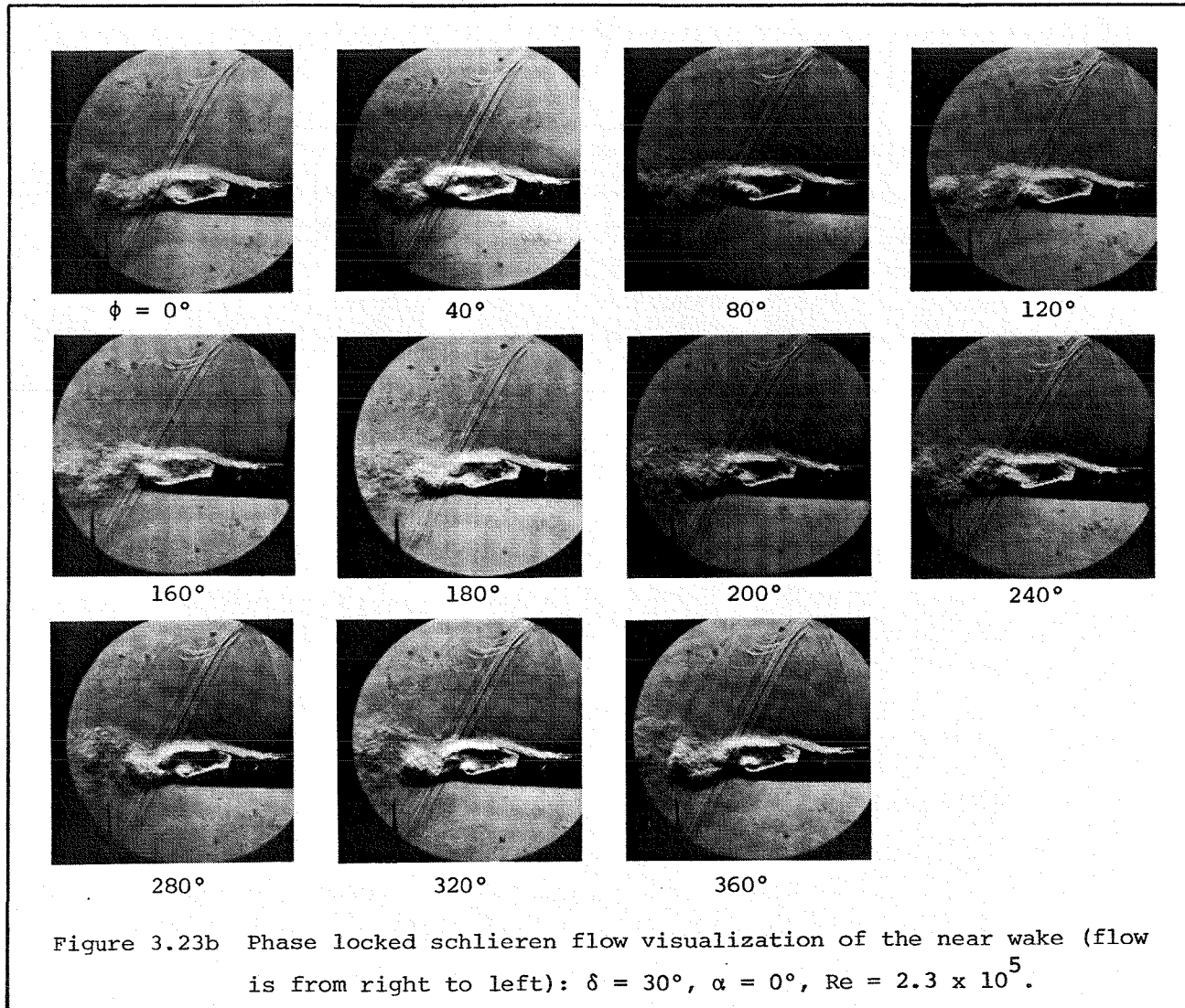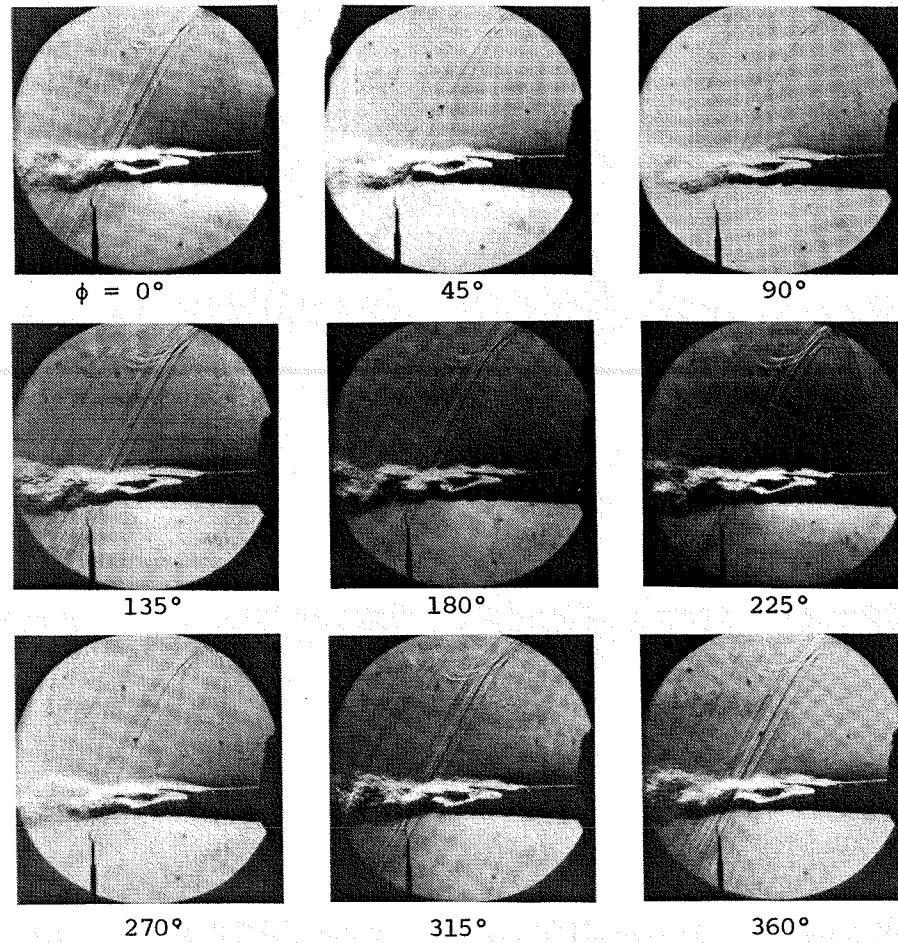
Figure 3.23c   Phase locked schlieren flow visualization of the near wake (flow is from right to left): $\delta = 15°$, $\alpha = 0°$, Re = 2.3 x 10^5.

End of Document